

Highlights

Relationship between Radar Cross Section and Optical Magnitude based on Radar and Optical Simultaneous Observations of Faint Meteors

Ryou Ohsawa, Akira Hirota, Kohei Morita, Shinsuke Abe, Daniel Kastinen, Johan Kero, Csilla Szasz, Yasunori Fujiwara, Takuji Nakamura, Koji Nishimura, Shigeyuki Sako, Jun-ichi Watanabe, Tsutomu Aoki, Noriaki Arima, Ko Arimatsu, Mamoru Doi, Makoto Ichiki, Shiro Ikeda, Yoshifusa Ita, Toshihiro Kasuga, Naoto Kobayashi, Mitsuru Kokubo, Masahiro Konishi, Hiroyuki Maehara, Takashi Miyata, Yuki Mori, Mikio Morii, Tomoki Morokuma, Kentaro Motohara, Yoshikazu Nakada, Shin-ichiro Okumura, Yuki Sarugaku, Mikiya Sato, Toshikazu Shigeyama, Takao Soyano, Hidenori Takahashi, Masaomi Tanaka, Ken'ichi Tarusawa, Nozomu Tominaga, Seitaro Urakawa, Fumihiko Usui, Takuya Yamashita, Makoto Yoshikawa

- In total, 331 meteors were detected simultaneously by radar and optically.
- A correlation between the radar cross section and the optical magnitude is firmly confirmed.
- The mass range of the meteor detected by MU radar is constrained to about 10^{-5} – 10^0 g.

Relationship between Radar Cross Section and Optical Magnitude based on Radar and Optical Simultaneous Observations of Faint Meteors

Ryou Ohsawa^{a,b}, Akira Hirota^c, Kohei Morita^c, Shinsuke Abe^c, Daniel Kastinen^d, Johan Kero^d, Csilla Szasz^d, Yasunori Fujiwara^{e,n}, Takuji Nakamura^f, Koji Nishimura^f, Shigeyuki Sako^a, Jun-ichi Watanabe^g, Tsutomu Aoki^b, Noriaki Arima^a, Ko Arimatsu^h, Mamoru Doi^{a,i}, Makoto Ichiki^a, Shiro Ikeda^j, Yoshifusa Ita^k, Toshihiro Kasuga^{l,g}, Naoto Kobayashi^{a,b}, Mitsuru Kokubo^k, Masahiro Konishi^a, Hiroyuki Maehara^m, Takashi Miyata^a, Yuki Mori^b, Mikiyo Morii^j, Tomoki Morokuma^a, Kentaro Motohara^a, Yoshikazu Nakada^a, Shin-ichiro Okumura^q, Yuki Sarugaku^l, Mikiya Satoⁿ, Toshikazu Shigeyamaⁱ, Takao Soyano^b, Hidenori Takahashi^{a,b}, Masaomi Tanaka^k, Ken'ichi Tarusawa^b, Nozomu Tominaga^{o,p}, Seitaro Urakawa^q, Fumihiko Usui^r, Takuya Yamashita^g, Makoto Yoshikawa^s

^a*Institute of Astronomy, Graduate School of Science, The University of Tokyo, 2-21-1 Osawa, Mitaka, Tokyo 181-0015, Japan*

^b*Kiso Observatory, Institute of Astronomy, Graduate School of Science, The University of Tokyo 10762-30, Mitake, Kiso-machi, Kiso-gun, Nagano 397-0101, Japan*

^c*Department of Aerospace Engineering, College of Science & Technology, Nihon University, 7-24-1 Narashinodai, Funabashi, Chiba 274-8501, Japan*

^d*Swedish Institute of Space Physics, Box 812, SE-981 28 Kiruna, Sweden*

^e*SOKENDAI (The Graduate University for Advanced Studies), 10-3 Midoricho, Tachikawa, 190-8518 Tokyo, Japan*

^f*National Institute of Polar Research, 10-3, Midori-cho, Tachikawa-shi, Tokyo 190-8518, Japan*

^g*National Astronomical Observatory of Japan, 2-21-1 Osawa, Mitaka, Tokyo 181-8588, Japan*

^h*Astronomical Observatory, Graduate School of Science, Kyoto University, Kitashirakawa-oiwake-cho, Sakyo-ku, Kyoto 606-8502, Japan*

ⁱ*Research Center for the Early Universe, Graduate School of Science, The University of Tokyo, 7-3-1 Hongo, Bunkyo-ku, Tokyo 113-0033, Japan*

^j*The Institute of Statistical Mathematics, 10-3 Midori-cho, Tachikawa, Tokyo 190-8562, Japan*

^k*Tohoku University, 6-3 Aramaki, Aoba, Aoba-ku, Sendai, Miyagi 980-8578, Japan*

^l*Department of Physics, Kyoto Sangyo University, Motoyama Kamigamo Kita-ku Kyoto 603-8555 Japan*

^m*Okayama Branch Office, Subaru Telescope, National Astronomical Observatory of Japan, NINS, Kamogata, Asakuchi, Okayama, Japan*

ⁿ*The Nippon Meteor Society*

^o*Kavli Institute for the Physics and Mathematics of the Universe (WPI), The University of Tokyo, 5-1-5 Kashiwanoha, Kashiwa, Chiba 277-8583, Japan*

^p*Department of Physics, Faculty of Science and Engineering, Konan University, 8-9-1 Okamoto, Kobe, Hyogo 658-8501, Japan*

^q*Japan Spaceguard Association, Bisei Spaceguard Center, 1716-3 Okura, Bisei, Ibara, Okayama 714-1411, Japan*

^r*Center for Planetary Science, Graduate School of Science, Kobe University, 7-1-48 Minatojima-Minamimachi, Chuo-Ku, Kobe, Hyogo 650-0047, Japan*

^s*Japan Aerospace eXploration Agency, 3-1-1 Yoshinodai, Chuo-ku, Sagami-hara, Kanagawa 252-5210, Japan*

Abstract

Radar and optical simultaneous observations of meteors are important to understand the size distribution of the interplanetary dust. However, faint meteors detected by high power large aperture radar observations, which are typically as faint as 10 mag. in optical, have not been detected until recently in optical observations, mainly due to insufficient sensitivity of the optical observations. In this paper, two radar and optical simultaneous observations were organized. The first observation was carried out in 2009–2010 using Middle and Upper Atmosphere Radar (MU radar) and an image-intensified CCD camera. The second observation was carried out in 2018 using the MU radar and a mosaic CMOS camera, Tomo-e Gozen, mounted on the 1.05-m Kiso Schmidt Telescope. In total, 331 simultaneous meteors were detected. The relationship between radar cross sections and optical V -band magnitudes was well approximated by a linear function. A transformation function from the radar cross section to the V -band magnitude was derived for sporadic meteors. The transformation function was applied to about 150,000 meteors detected by the MU radar in 2009–2015, large part of which are sporadic, and a luminosity function was derived in the magnitude range of -1.5 – 9.5 mag. The luminosity function was well approximated by a single power-law function with the population index of $r = 3.52 \pm 0.12$. The present observation indicates that the MU radar has capability to detect interplanetary dust of 10^{-5} – 10^0 g in mass as meteors.

Keywords: meteors, meteoroids, interplanetary medium

1. Introduction

Asteroids and comets are relatively active members in the solar system. They sometimes show cometary activi-

February 9, 2021

Email address: ohsawa@ioa.s.u-tokyo.ac.jp (Ryou Ohsawa)

ties in the vicinity of the Sun and abruptly eject dust by collision or rapid rotation. The Earth is surrounded by small dust particles generated by such events, which are widely referred to as the interplanetary dust. The mass and size distributions of the interplanetary dust provide important information to understand the origin and evolution of the solar system.

The interplanetary dust grains are steadily colliding with the Earth. The amount of the grains incoming to the Earth is estimated to be about $5\text{--}300\times 10^3$ kg per day (Plane, 2012), which largely consists of grains of $10^{-9}\text{--}10^{-2}$ g in mass (Flynn, 2002). The interplanetary dust grains smaller than 10^{-6} g have been intensively examined by direct dust detectors onboard spacecrafts (Grün et al., 1985; Gruen et al., 1992; Gurnett et al., 1997; Szalay et al., 2013). A detector with a much larger collecting area is, however, required to investigate larger dust grains.

Observing meteors is a method to use the Earth's atmosphere as a huge detector. Atoms and molecules in the atmosphere are ionized and excited by an interplanetary dust grain which enters the atmosphere. These processes are interpreted by the theory of thermal ablation (Baldwin and Sheaffer, 1971; Ceplecha et al., 1998; Popova, 2004). Part of the kinetic energy is converted into light. The fraction of the energy converted into light to the lost kinetic energy is called *the luminous efficiency*, which is a key physical quantity to determine the brightness of the meteor. Part of the kinetic energy is also used to ionize surrounding atmospheric molecules. The probability that an atmospheric atom is ionized on a deposition of a single atom from the meteoroid is called *the ionization coefficient*, which determines the electron density of the meteor. There are several attempts to constrain these coefficients observationally (e.g., Verniani, 1965), experimentally (e.g., Boitnott and Savage, 1972; Friichtenicht and Becker, 1973; Thomas et al., 2016), and theoretically (e.g., Jones, 1997). Radar and optical observations are important to constrain these quantities.

Radar meteors corresponding to extremely faint optical meteors have been detected in the meteor head echo observations with high power and large aperture radar systems such as the European Incoherent Scatter (EISCAT) radars, Advanced Research Projects Agency Long-Range Tracking And Instrumentation Radar (ALTAIR), Middle-and-Upper Atmosphere radar (MU radar), the Middle Atmosphere ALOMAR Radar System (MAARSY), Southern Argentine Agile MEteor Radar (SAAMER), and Poker Flat Incoherent Scatter Radar (PFISR) (Pellinen-Wannberg and Wannberg, 1994; Close et al., 2000; Sato et al., 2000; Kero et al., 2011; Schult et al., 2017; Fentzke et al., 2009; Sparks et al., 2009; Janches et al., 2014, 2015, 2019). Pellinen-Wannberg et al. (1998) estimated that EISCAT is able to detect meteors as faint as 10 mag based on the measurements of cross sections and event rates. Thanks to the advances of digital video cameras, such faint meteors have since then been detected optically. Meteors brighter than 4 mag are routinely collected by large meteor sur-

vey networks (Jenniskens, 2017), such as Cameras for All-sky Meteor Surveillance (CAMS; Jenniskens et al., 2011), European viDeo MeteOr Network Database (EDMOND; Kornos et al., 2013), and SonotaCo network (Kanamori, 2009). Recently, high-sensitive optical camera systems make it possible to observe meteors as faint as ~ 10 mag in the optical regime (Nishimura et al., 2001; Weryk et al., 2013; Ohsawa et al., 2019).

Since every observation method is subject to biases and errors, simultaneous observations of the same meteors using different methods are important. Part of previous simultaneous observations are described here. Fujiwara et al. (1995) carried out simultaneous observations with the MU radar and three video cameras with image intensifiers. In two observation runs, they detected 19 simultaneous meteors and suggested a log-linear relationship between the radar received power and the optical magnitude for Geminids. Nishimura et al. (2001) detected 35 simultaneous meteors during two nights using the MU radar and an image-intensified CCD video camera. They showed that the radar received power changed partly in synchronization with the optical brightness. They also confirmed a log-linear relationship between the radar received power and the optical magnitude for sporadic meteors. Michell (2010) detected seven meteors in optical out of 338 meteors observed with PFISR, and confirmed that a similar positive correlation between the optical brightness and the back-scattered radar power. Using a combination of SAAMER and an EMCCD video camera, Michell et al. (2015) obtained 6 meteors simultaneously by radar and optically and showed that the meteoroid masses independently estimated from the radar and optical observations were roughly consistent with each other. Michell et al. (2019) carried out optical and dual-frequency radar observations with the Arecibo radar and an EMCCD camera. In total, 19 meteor events were detected simultaneously in the three methods. No apparent correlation between the optical mass and the radar signal-to-noise ratios was, however, confirmed. Since not a small fraction of the meteors were detected in side lobes, they presumed that the radar cross sections could be underestimated, resulting in a possible artificial bias. Campbell-Brown et al. (2012) carried out observations with EISCAT and two image-intensified CCD video cameras and detected 4 meteors whose orbits were determined both by radar and optically. They confirmed that the photometric and ionization masses were consistent within estimated errors. Weryk and Brown (2013, 2012) used the Canadian Meteor Orbit Radar (CMOR) and multiple image-intensified CCD video cameras and detected about ~ 500 simultaneous meteors in the magnitude range of about 0–5 mag. They derived the relationship between the electron line density and the photon radiant power. The dependency of the ionization coefficient to the luminous efficiency ratio on the speed of meteors was observationally constrained. The luminous efficiency they derived indicated that the meteoroid mass flux in the range $10^{-5}\text{--}10^{-2}$ g could be lower than previously es-

timated. [Brown et al. \(2017\)](#) carried out observations with MAARSY and two image-intensified video cameras. They detected more than 100 simultaneous meteors whose orbits were constrained both by radar and optically. The magnitudes of the detected meteors ranged from 0–7 mag. They found a clear trend where brighter meteors showed higher peak radar cross sections. More complete overviews are found in [Weryk and Brown \(2012, 2013\)](#) and [Brown et al. \(2017\)](#).

Although there have been a number of radar and optical simultaneous observations in literature, meteors fainter than ~ 6 mag have not been fully investigated. This is partly because the performances of optical camera systems are limited. A combination of a large aperture, high-speed and continuous imaging, and a large field-of-view is required to detect faint meteors optically. Recently, [Ohsawa et al. \(2019\)](#) carried out observations of meteors as faint as ~ 10 mag with a mosaic CMOS camera, Tomo-e PM, mounted on the 1.05-m Kiso Schmidt telescope. A combination of a large and wide-field telescope and a mosaic CMOS camera is preferable to detect faint meteors. Here, we report two simultaneous observations of faint sporadic meteors. The observations are intended to confirm the trends between the radar cross section in the meteor head echo observation and the optical magnitude suggested in previous studies ([Nishimura et al., 2002](#); [Michell et al., 2015](#); [Brown et al., 2017](#)) with a large number of samples and a wide magnitude range. In the first observation run, observations were carried out with the MU radar and an image-intensified CCD video camera in 2009–2010. The second observation run were carried out with the MU radar and Tomo-e Gozen, which is a successor of Tomo-e PM. The paper is organized as follows; Details of the observations are described in Section 2. Statistical properties of detected meteors are presented in Section 3. In Section 4, the relationship between the radar cross section and the optical brightness and the luminosity function of sporadic meteors are discussed, and then Section 5 summarizes this paper.

2. Observations

2.1. Observations with the MU radar and Intensified CCD camera

The first observation run was carried out in 2009 and 2010 (hereafter, referred as to ICCD09). Specifications of the observations are summarized in Table 1. We had several observations in 2009 and 2010. Radar observations were carried out with Middle and Upper Atmosphere Radar (hereafter, MU radar) in the Shigaraki MU Observatory¹ of Research Institute for Sustainable Humanosphere (RISH), Kyoto University. The MU radar was operated

¹Shigaraki MU Observatory is located at $+34^{\text{d}}51^{\text{m}}14^{\text{s}}.5\text{N}$ and $+136^{\text{d}}06^{\text{m}}20^{\text{s}}.24\text{E}$ (WGS84).

in the general head echo mode ([Kero et al., 2011](#)). Optical observations were carried out with an image-intensified CCD camera made by Hamamatsu equipped with a Canon 200 mm F/1.8 lens. The optical camera system was set up in Shigaraki. The camera was pointed toward zenith and continuously monitored the sky at 29.97 Hz. GPS time stamps were imprinted in the video data.

The radar data were reduced using a standard data reduction process of the MU radar ([Kero et al., 2011, 2012a,b](#)). The three dimensional trajectory and the radar cross section (RCS) along the trajectory of each meteor were obtained. Meteors in the optical data were detected with a time shifted motion capture software, UFOCapture². The optical trajectories and the magnitudes of the meteors were derived with a post processing tool, UFOAnalyzer³.

2.2. Observations with the MU radar and Tomo-e Gozen

The second observations were carried out in April, 2018 (hereafter, referred as to KISO18). Radar observations were also carried out with the MU radar in the same setting as in ICCD09. Optical observations were carried out with a mosaic CMOS camera, Tomo-e Gozen, mounted on the 1.05-m Schmidt Telescope in Kiso Observatory⁴ of the Institute of Astronomy, the University of Tokyo. Specifications of the observations are summarized in Table 2. Tomo-e Gozen is equipped with 84 CMOS image sensors of 2000×1128 pixels in size. The field-of-view is, in total, as large as about 20 sq. degree, and Tomo-e Gozen is able to monitor the sky up to at 2 Hz ([Sako et al., 2016, 2018](#); [Kojima et al., 2018](#)). The readout of the image sensor is synchronized with the GPS time and the time stamp of Tomo-e Gozen is as accurate as 0.2 ms ([Sako et al., 2018](#)). Observations are carried out in a clear filter and a nominal limiting magnitude for stars is about 18 mag, which is corresponding to about 12 mag for meteors ([Ohsawa et al., 2019](#)). At the time of the observations, only one quadrant of the camera was available and one sensor was not operating. Thus, the observations were carried out with 20 CMOS sensors (~ 4.8 sq. degree in total). The Kiso Schmidt telescope was pointed toward the sky 100 km above the MU radar. Since the telescope tracked the sky, the direction of the telescope was adjusted every 3 minutes. Thus, the length of each video is 3 minutes. Kiso Observatory is located about 173 km distant from the Shigaraki MU Observatory. The elevation angle of the telescope was about 30° and the distance between the telescope and the volume monitored by the MU radar was about 200 km.

The radar data were reduced in the same manner as in ICCD09. The three dimensional trajectory and the RCS of

²UFOCaptrueV2 (ver 2.24) in http://sonotaco.com/soft/e_index.html

³UFOAnalyzerV2 (ver 2.44) in http://sonotaco.com/soft/e_index.html

⁴Kiso Observatory is located at $+35^{\text{d}}47^{\text{m}}38^{\text{s}}.7\text{N}$ and $+137^{\text{d}}37^{\text{m}}42^{\text{s}}.2\text{E}$ (WGS84).

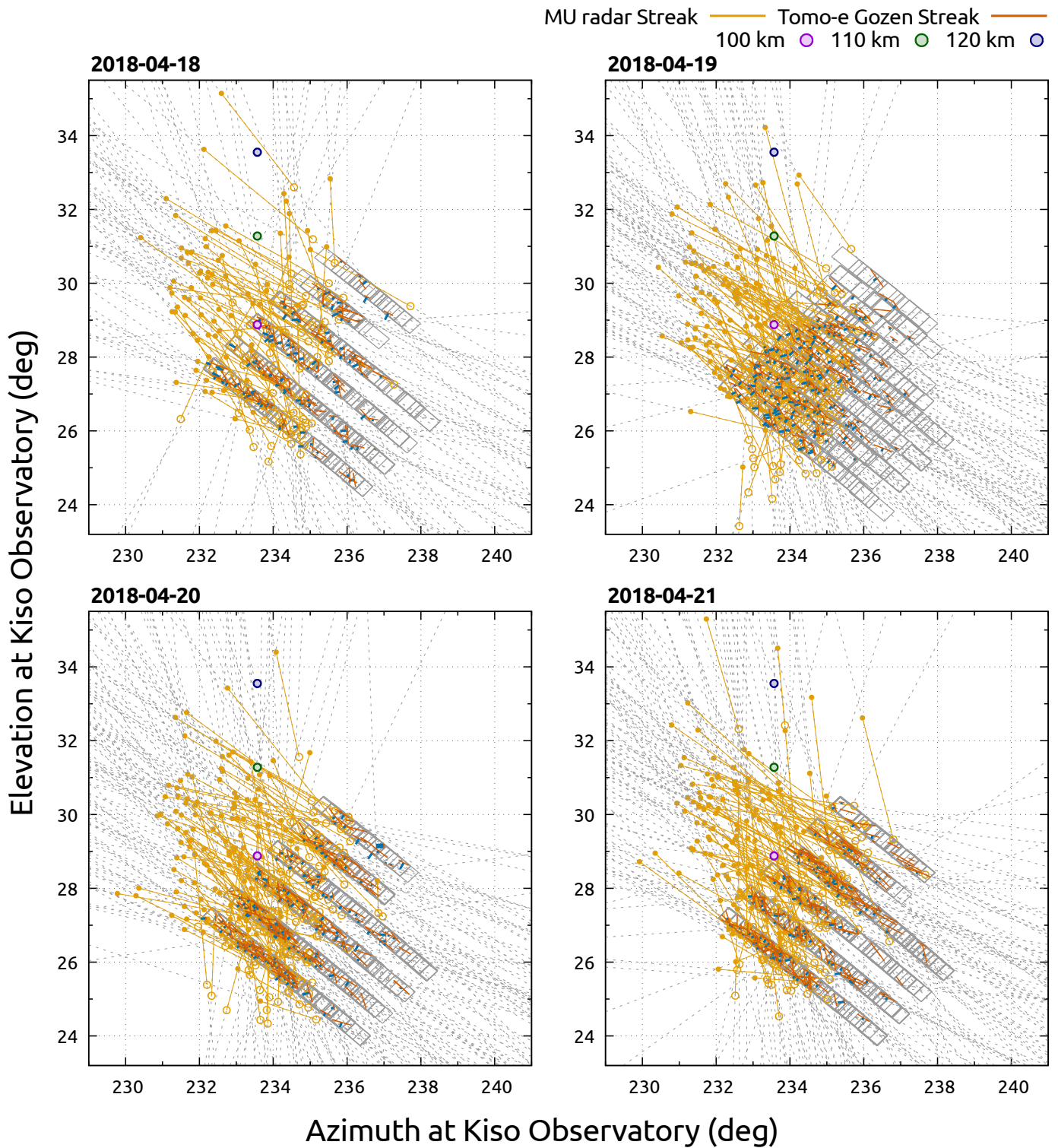


Figure 1: The meteors detected in KISO18 are projected onto the sky from Kiso Observatory in the elevation and azimuth coordinates. Each panel illustrates the meteors detected in a night. The orange segments indicate the meteors detected by the MU radar; The filled and empty circles are, respectively, the first and last detection points. The gray dashed lines are the extensions of the MU trajectories for reference. The gray rectangles are the fields-of-view of Tomo-e Gozen. The red segments indicate the meteors detected by Tomo-e Gozen. The blue segments indicate the distances between the meteor segments detected by the MU radar and Tomo-e Gozen. The violet, green, and navy circles respectively indicate the center of the field-of-view of the MU radar at 100, 110, and 120 km in altitude.

Table 1: Summary of Observations with the MU radar and ICCD camera in 2009–2010

Date	Sep. 24–26, Oct. 19–21, Nov. 8, and Dec. 13–14 in 2009 Mar. 11, Aug. 12, Sep. 13, and Dec. 14 in 2010
Radar System	Middle and Upper Atmosphere Radar (46.5 MHz)
Optical System	Canon 200 mm F/1.8 and Hamamatsu CCD camera (ORCA-05G)
Video Frame Rate	29.97 Hz
Field of View	$\sim 6^\circ$ in diameter (radar), $9.9^\circ \times 10.9^\circ$ (optical)

Table 2: Summary of Observations with the MU radar and Tomo-e Gozen in 2018

Date	Apr. 18–22 in 2018 (11:00–20:00 UT, 36 hours in total)
Radar System	Middle and Upper Atmosphere Radar (46.5 MHz)
Optical System	1.05-m Kiso Schmidt telescope and Tomo-e Gozen (Q1)
Video Frame Rate	2.0 Hz
Field of View	$\sim 6^\circ$ in diameter (radar), $20 \times 39.7' \times 22.4'$ (optical)

each meteor were obtained. The optical data were reduced in a standard astronomical data reduction procedure for imaging observations: a dark frame was subtracted and a flat frame correction was applied. Meteors in the optical video data were extracted with an algorithm based on the Hough transformation (Ohsawa et al., 2016, 2019). The detected events are summarized in Figure 1. The meteors detected by the MU radar are shown by the orange segments, while those detected by Tomo-e Gozen are shown by the red segments. The gray rectangles indicate the fields-of-view of Tomo-e Gozen. A number of rectangles appear in Figure 1 since the telescope was moved frequently. The violet, green, and navy circles in Figure 1 indicate the center of the field-of-view of the MU radar at different altitudes for reference. This indicates that the fields-of-view of Tomo-e Gozen were, however, slightly displaced due to a miscalculation.

2.3. Archival Observations from the MU radar Meteor Head Echo database

Meteors detected by the MU radar were retrieved from an archival data, in order to discuss the luminosity function of faint meteors. Part of data were already published in (Kero et al., 2012a, 2011) and available in the MU Radar Head Echo Database (MURMHED). All the data were reduced along with Kero et al. (2012b). The observations were carried out during 2009–2015 and the total observing time was 845.8 hour. The archive contains 157043 meteor events in total. The contributions from meteor showers were removed based on the D-criterion⁵, which is a criterion to determine whether a meteor belongs to a stream or not (Southworth and Hawkins, 1963). The threshold of the D-criterion was set to 0.2. This threshold is relatively weak compared to previous studies which identify meteor showers by the D-criterion (e.g., Jenniskens and Nénon, 2016),

but reasonable to roughly estimate the contributions from meteor showers (Andreić et al., 2014; Šegon et al., 2014; Gural et al., 2014; Andreić et al., 2013). Some sporadic meteors may be wrongly removed due to the weak threshold, but the result will not be affected. The removed meteors were mainly composed of Geminids (1034), Orionids (2049), and η Aquariids (1900). Finally, 150080 meteors were extracted as sporadic meteors. The archive was compiled with several campaign observations. The number of events per month is listed in Table 3. The table indicate that the observations were biased toward meteors observed in October and December.

3. Results

3.1. Simultaneous Meteors of ICCD09

We define “a simultaneous meteor” as a meteor observed both by radar and optically. In case of ICCD09, simultaneous meteors were identified based on the trajectories and timings of meteors. When meteors were detected both by radar and optically and the time separation was within 0.5 s, the meteors were considered as identical. Finally 145 meteors were identified as the simultaneous events.

Some observations were scheduled when meteor showers were active. Meteors belonging to showers were removed based on the D-criterion. The threshold for the D-criterion was set to 0.2 similarly as described above. The present dataset possibly contained 5 Southern Taurids, 13 Geminids, 17 Orionids, 1 Andromedids, 2 December Monocerotids, 1 Comae Berenicids, 2 ε Geminids, 16 η Aquariids, 1 October Capricornids, and 1 November Orionids. The remaining 103 meteors were considered to be sporadic. In the following sections, the 103 sporadic meteors were investigated.

The brightness of the ICCD09 meteors were calibrated against the V-band magnitudes in SKY2000 catalog version 4 (Myers et al., 2001) using UFOAnalyzer. The correction of the color term was not applied. Note that the

⁵The calculation was based on the orbital elements of the 112 established meteor showers issued in the IAU Meteor Data Center on February 17, 2020.

Table 3: The Number of Sporadic Meteor Events in MURMHED

Year	Jan.	Feb.	Mar.	Apr.	May	Jun.	Jul.	Aug.	Sep.	Oct.	Nov.	Dec.
2009	—	—	—	—	—	3819	5465	—	5419	9071	4925	4632
2010	3398	2788	2000	2205	2479	3064	3570	8520	4441	21467	4856	8314
2011	—	—	—	—	—	—	—	—	—	6087	—	—
2012	—	—	—	—	—	—	—	—	—	10930	—	—
2013	3298	2231	1708	—	—	—	—	—	—	—	—	13332
2014	3300	—	—	—	136	—	—	—	—	—	—	6477
2015	—	—	—	2148	—	—	—	—	—	—	—	—
total	9996	5019	3708	4353	2615	6883	9035	8520	9860	47555	9781	32755

derived magnitudes could be affected by an amount depending on the unknown spectral character of the meteors. The light curve of each meteor was derived. About 20% of the meteors showed light bursts with amplitudes of larger than 1.5, mag in their light curves, possibly attributed to fragmentation. Such sudden bursts are not necessarily accompanied by variations in the RCS (e.g., [Brown et al., 2017](#)). The meteors obtained in KISO18 were rarely affected by such bursts since they were observed in a narrow fields-of-view. To enable a fair comparison with the magnitude in KISO18, the magnitude averaged over the streak was adopted as the representative value of each meteor, instead of the peak magnitude, since the latter could be affected by fragmentation. Since the bursts were sufficiently short, the variability in the brightness had little effect on the average brightness values. Finally, the observed magnitudes were converted into the meteor absolute magnitudes.

3.2. Simultaneous Meteors of KISO18

To extract simultaneous meteors, we first sifted the optical meteors detected within ± 1 frames (1.5 s) of the time stamp of each meteor detected by radar. Then, the meteors detected by radar were projected onto the sky from Kiso Observatory (Figure 1). The candidates of the simultaneous meteors were selected based on the differences in direction and the separations; The angle between the radar (orange) and optical (red) trajectories should be smaller than 2.5° and the separation angle of the two trajectories (the blue segment in Figure 1) should be smaller than 0.25° . When the same meteor was detected in multiple detectors, the brightest segment was adopted as the representative one. The total number of unique simultaneous meteors was 485 in the four nights. As shown in Figure 1, the pointing of the telescope was displaced. The radar and optical observations sometimes traced completely different portions of the trajectory. The magnitudes of such meteors could be erroneous. Thus, we removed about 250 simultaneous meteors whose optical trajectories were not completely covered by the radar observations. A possible contribution from meteor showers were removed based on the D-criterion. In total, 5 meteors were removed. Finally, the sample size was reduced to 228, which accounted for

about 8% of the total number of the meteors whose radar trajectories crossed the fields-of-view of Tomo-e Gozen. In the following sections, the 228 simultaneous sporadic meteors were investigated.

The meteors in KISO18 were observed at 2 Hz. Thus, the meteors were captured as streaks. We calculated the magnitudes of the meteors, following the method used in [Iye et al. \(2007\)](#), to derive the brightness of the meteors from the detected streaks. The brightness of the meteor was estimated by $I_v v T$, where I_v is the line intensity averaged along the streak, v is the angular velocity of the meteor, and T is the exposure time of each video frame. In [Iye et al. \(2007\)](#), the meteor speeds v were uniformly assumed to be 10° s^{-1} . The magnitudes of meteors were also derived based on the same assumption in [Ohsawa et al. \(2019\)](#). This assumption was a major source of the uncertainty in those studies. In the KISO18 observation, the projected motion of each meteor was directly derived from the MU radar observation. The magnitudes in the present research were little affected by the uncertainty in the meteor speed. The magnitudes of the meteors were first calibrated against the V-band magnitudes of the UCAC4 catalog ([Zacharias et al., 2013](#)). The color term correction was not applied. Note that the derived magnitudes could be affected by an amount depending on the unknown spectral character of the meteors. Then, the magnitudes were finally converted into the meteor absolute magnitudes using the distance between the telescope and the meteors.

3.3. Statistics of Simultaneous Meteors

The distributions of the absolute magnitude is shown in Figure 2. The top panel shows the distribution of ICCD09, while the bottom panel does that of KISO18. The brightest meteor in ICCD09 was 1.4 mag, while the faintest meteor was 10.0 mag. The magnitudes at 25-, 50-, and 75-percentiles were 5.0, 6.1, and 7.2 mag, respectively. The brightest meteor in KISO18 was about 2.8 mag, while the faintest meteor was 11.1 mag. The magnitudes at 25-, 50-, and 75-percentiles were 7.4, 8.1, and 8.6 mag, respectively. The detected meteors in KISO18 were typically about 1.8 mag fainter than those in ICCD09, in spite of the larger distance between the radar and optical observation sites. This is simply attributed to the high sensitivity

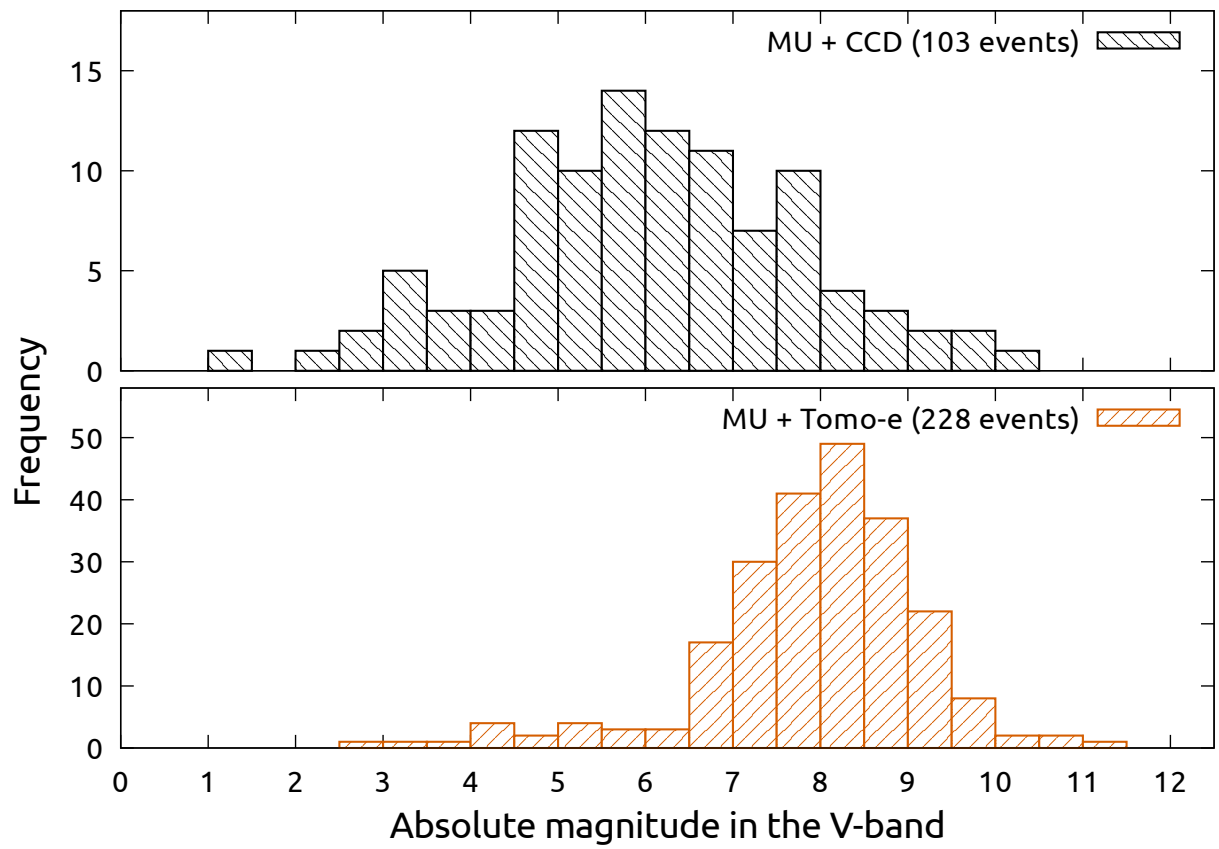


Figure 2: Magnitude distributions of the meteors simultaneously detected by radar and optically. The top panel shows the magnitude distribution of the observations in 2009–2010 (ICCD09), while the bottom panel illustrates that of the observations in 2018 (KISO18).

of Tomo-e Gozen.

The top panel of Figure 3 displays the altitudes of the meteors against the optical absolute magnitudes. No apparent dependency of the altitude on the optical magnitude was recognized. But this does not mean the distribution of the meteoroid mass was uniform along the altitude. It should be noted that a limiting meteoroid mass is smaller at a higher altitude for a magnitude-limited sample (e.g., see Figure 4 in Ceplecha et al., 1998). The altitudes of the KISO18 meteors are generally lower than those of the ICCD09 meteors. As shown in Figure 1, the pointing of the telescope in KISO18 was displaced downward in elevation. The fields-of-view of Tomo-e Gozen were set below about 30° in elevation, corresponding to about 100 km in altitude above the MU radar. Since the differences between the highest and lowest altitudes is typically about 10 km in Figure 3, the meteors below 110 km were selectively detected as simultaneous meteors in KISO18. Thus, the difference in the altitude distributions is explained by the observation bias. Consequently, the present samples contained few meteors which were fainter than about 7 mag and whose altitudes were higher than 100 km. The geocentric velocities are plotted against the optical magnitudes in the bottom panel of Figure 3. No apparent trend is confirmed. The distribution of the geocentric velocity is bimodal.

Figure 4 shows the distribution of the meteor radiant in the Hammer projection of the ecliptic latitude and Sun-centered ecliptic longitude coordinates. The meteors whose geocentric velocity is faster than 45 km s^{-1} are shown by the orange symbols. The distribution of the faster population is consistent with the apex sources (e.g., Hawkins, 1956a), while the slower populations are possibly attributed to the antihelion and north toroidal sources (e.g., Hawkins, 1956a; Štohl, 1968). No significant concentration is found in Figure 4, suggesting that possible contributions from meteor showers were successfully removed.

Figure 5 shows the optical absolute magnitude against the RCS, which is the value at the maximum signal-to-noise ratio (SNR) along the whole radar trajectory. On the other hand, the brightest magnitudes were independently measured in the optical observations. Thus, the section where the RCS was measured and the section where the optical brightness was measured could be different. A possible uncertainty due to this time difference is discussed later. The data of ICCD09 and KISO18 seem to follow the same trend, where the optical magnitude became brighter as the RCS became larger. The trend was approximated by a linear regression line. Since there was large scatter in Figure 5, trial regression lines were calculated both in terms of the RCS and the magnitude via a least-square method and then the line with the averaged slope was adopted as the representative regression line:

$$M_V = -(0.169 \pm 0.006) \times A + (4.43 \pm 0.13), \quad (1)$$

where M_V is the meteor absolute magnitude in the V -band

and A is the radar cross section in units of dBsm (decibel relative to 1 m^2). The representative regression line is shown by the blue dashed line in Figure 5. The uncertainties were estimated by the bootstrapping method. It should be noted that, since the color-term correction was not applied, the present result could suffer from a systematic bias due to different spectral responses of the cameras. Such a possible bias was not taken into account in the uncertainties in Equation (1).

4. Discussion

4.1. The relationship between the RCS and the optical magnitude

Figure 5 indicates that the data follow a single and linear relationship. No apparent deviation from the regression line is confirmed. The dependence of the relationship on the meteor speed is investigated by splitting the sample into the fast ($> 45 \text{ km s}^{-1}$) and slow ($\leq 45 \text{ km s}^{-1}$) members, but no significant difference is confirmed. This suggests that sporadic meteors from the apex, antihelion, and north toroidal sources follow the same relationship.

The scatter in Figure 5 is much larger than the errors of the data. This may in part be due to the fact that the sections where the RCS and the optical magnitude were measured were close but not exactly the same. Both the RCS and the optical brightness are variable along the trajectory (e.g., see Figure 11 in Brown et al., 2017). The variation in the RCS and the optical brightness should contribute to the scatter. Especially, fragmentation may cause a sudden increase in the RCS and optical brightness, but the impacts of the fragmentation on the RCS and the magnitude are not necessarily the same (Campbell-Brown et al., 2013; Brown et al., 2017). Fragmentation may cause pulsations in head echo RCS curves due to interference from two or more scattering centers (Kero et al., 2008), while the luminosity produced is assumed to be proportional to the total kinetic energy lost by the meteoroid (Campbell-Brown et al., 2013), thus proportional to the increased cross-sectional area to mass of the fragments. Weryk et al. (2013) reported that 17% of meteors detected by the CAMO system showed clear signs of fragmentation. Similarly, a significant fraction of the data in Figure 5 could be affected by fragmentation. This may partly explain the large scatter: ~ 2 mag in the optical magnitude and ~ 10 dBsm in the RCS, which are roughly consistent with the changes caused by the fragmentation. Several studies have suggested that the ratio of the emission to ionization coefficients depends on the velocity (Saidov and Simek, 1989; Jones, 1997; Weryk and Brown, 2013). This dependence may contribute to the scatter, but the difference in the distributions was not confirmed in the present data. A variety of chemical compositions may contribute to the scatter. Spectroscopic observations are required to confirm it.

Although the origin of the large scatter has not been identified, we tentatively conclude that the relationship

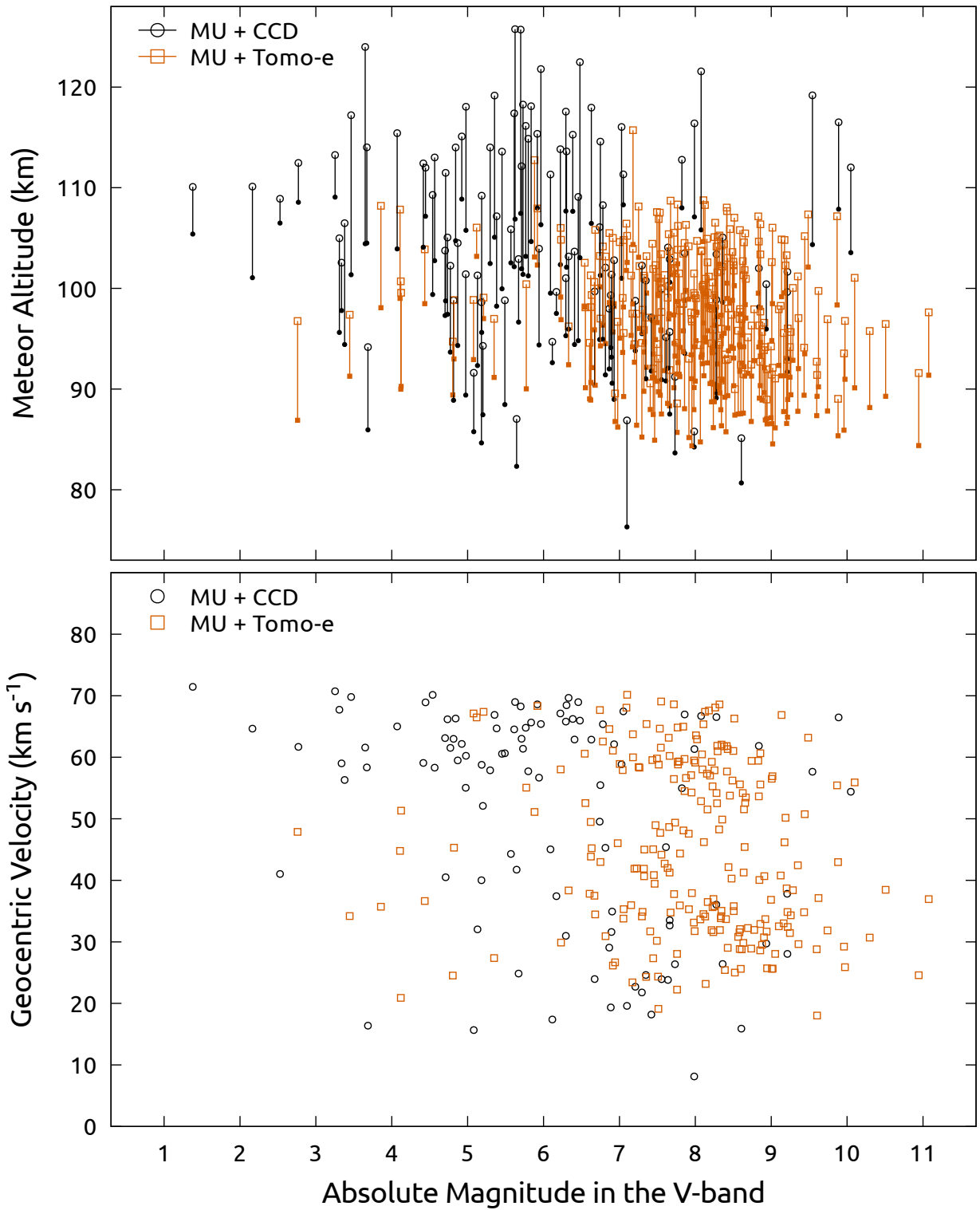


Figure 3: The altitude and the geocentric velocity are shown against the optical magnitude in the V -band. The data of ICCD09 are shown by the black circle symbols, while those of KISO18 are shown by the red square symbols. The top panel illustrates the observed heights in km. The empty and filled symbols are respectively the highest and lowest altitudes measured by the MU radar. The geocentric velocity in km s^{-1} is shown in the bottom panel.

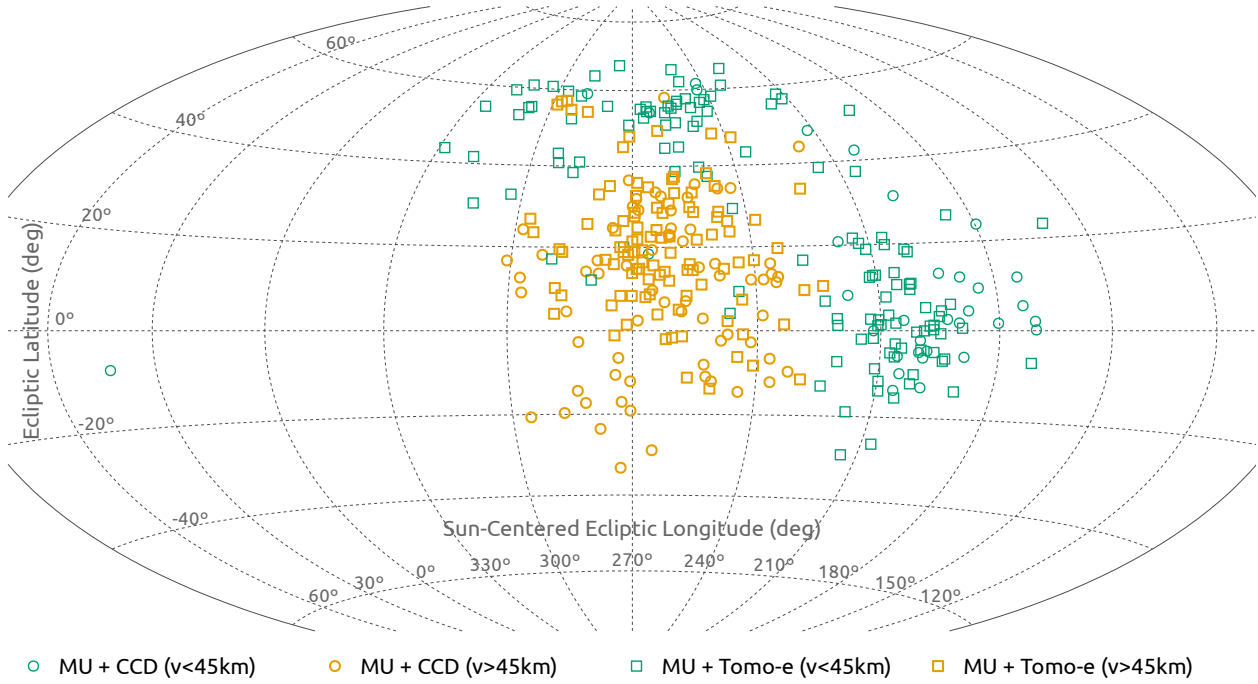


Figure 4: The radiant distribution of the simultaneous meteors in the Sun-centered Ecliptic coordinates. The data of ICCD09 are shown by the circle symbols, while those of KISO18 are shown by the square symbols. The meteors whose geocentric velocities are faster than 45 km s^{-1} are shown in orange, while the meteors slower than 45 km s^{-1} are shown in green.

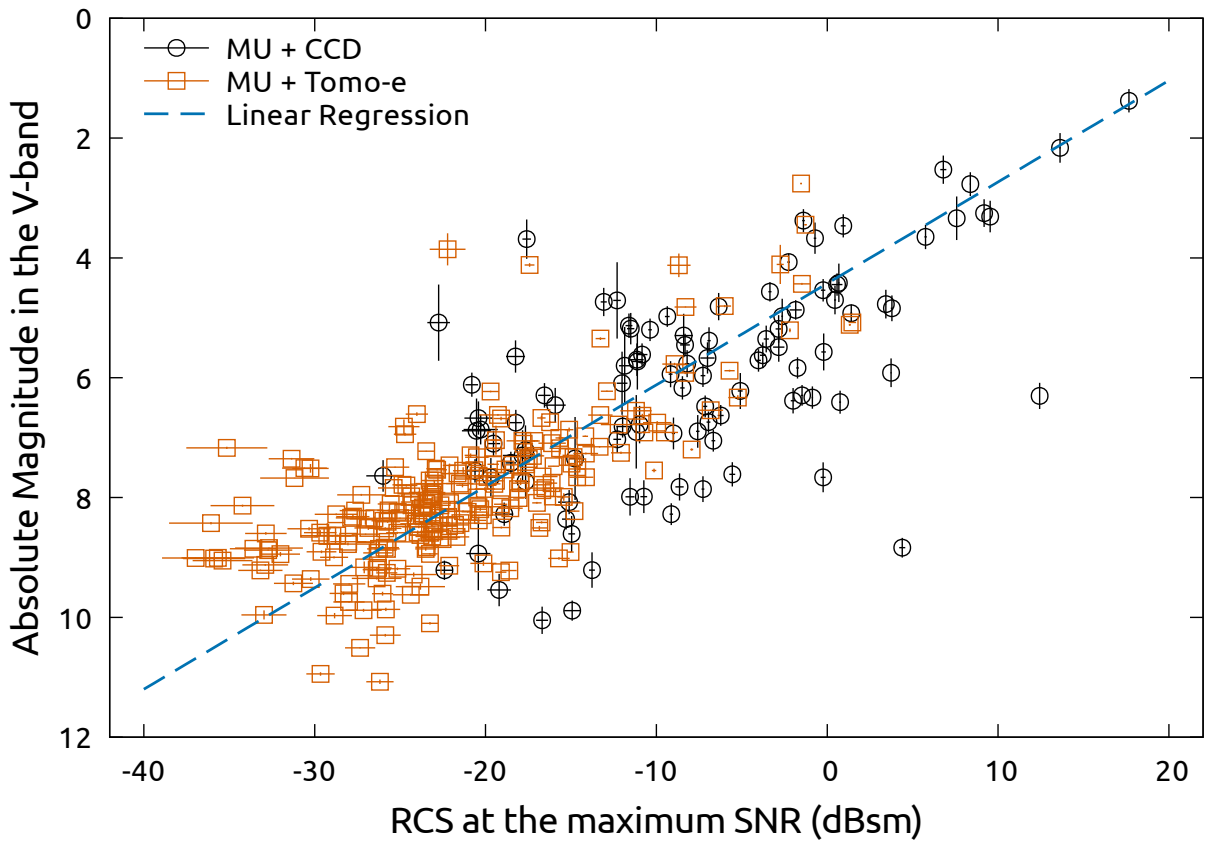


Figure 5: The relationship between the radar cross section and the optical absolute magnitude in the V-band. The meteors of ICCD09 and KISO18 are shown by the black circle and red square symbols, respectively. The blue dashed line indicates the linear regression line.

between the RCS and the optical magnitude is well approximated by a linear function over a magnitude range of about 1–9 mag, but we do not exclude the possibility that any deviations from the linear relationship are hidden within the scatter. The possibility that the relationship is variable or there are multiple relationships is not excluded as well. The scatter can be attributed to possible variations in the relationship. In such a case, the present relationship is considered to be an averaged one over the current dataset. Note that the uncertainties in Equation (1) were derived with the assumption that the relationship is unique among the dataset, where the variation in the relationship was not taken into account.

A scattering model of a head echo plasma was developed by Close et al. (2004), which provided a method to estimate the meteoroid mass, referred as to *scattering mass*, from the head echo RCS (Close et al., 2005). Close et al. (2007) investigated the dependence of the head echo RCS on the electron line density (q), the scattering mass (m_s), the velocity (v), and the mean-free-path (l). A multivariate regression provided a relationship $q \propto m^{1.08} v^{3.09} l^{-0.11}$ and the head echo RCS (A) was approximated as $A \propto q^{1.05} \propto m_s^{1.05 \times 1.08}$. Here, we simply assume that the brightness of the meteor approximately follows $I \propto m_p$, where m_p is the photometric mass. By equating m_s with m_p , a relationship between the magnitude (M_V) and the head echo RCS is derived: $M_V = -0.22A + \text{const}$. The slope of this relationship is similar to but steeper than the present result. This may implicate that the dependence of the head echo RCS is larger than suggested in Close et al. (2007), or that the dependence of the optical brightness on the meteoroid mass is smaller. Note that the comparison above is highly simplified. A model calculation which evaluates the head echo RCS and the optical brightness simultaneously is required.

Nishimura et al. (2001) provided a conversion function from the optical magnitude to the radar received power in units of dB, where the optical magnitude decreased by about 0.3 mag when the radar power increased by 1 dB, corresponding to the slope of -0.3 . Since their result was derived from 20 simultaneous meteors, the slope could be affected by a considerable uncertainty. We estimate the uncertainty of the slope in case that the sample size is limited to 20 using a bootstrap sampling method: 20 meteors are randomly selected from the present 332 simultaneous meteors and a slope is derived by a least-square method. This process is repeated 1,000 times. Then, the posterior probability distribution of the slope is approximated by the distribution of the derived slopes. The 95% confidence interval is $(-0.13, -0.32)$. Thus, we presume that the present slope is marginally consistent with that in Nishimura et al. (2001). Brown et al. (2017) presented the relationship between the RCS the optical magnitude based on their 105 simultaneous meteors (*see*, Figure 9). While no regression line was presented, the optical magnitude decreased roughly by 0.05–0.16 mag when the RCS increased by 1 dB. The slope seems smaller than that of

the present result. The optical magnitudes ranged over roughly 0–6 mag in Brown et al. (2017), while only a handful of meteors were detected in this magnitude range in the present work. The possibility that the relationship changes around 5 mag is not excluded.

The data of ICCD09 and KISO18 were obtained using different systems and on different days. Equation (1) could suffer from systematic errors, such as the difference in spectral response and the annual variations. Further observations are required to evaluate the uncertainty of Equation (1). The data of KISO18 were obtained in only four nights. This suggests that the combination of the MU radar and Tomo-e Gozen is promising to investigate the annual and diurnal variations in the relationship between the RCS and the optical magnitude.

4.2. Meteor Luminosity Function of the MU radar Meteor Head Echo Database

A luminosity function of visible meteors has been widely approximated by a power-law function (Hawkins and Upton, 1958):

$$\log_{10} N(<M) = \log_{10} N_0 + M \log_{10} r, \quad (2)$$

where $N(<M)$ and N_0 are the event rates of meteors brighter than M -th and zero-th magnitudes, respectively, and r defines the slope of the distribution, generally referred as to *the population index*. Cook et al. (1980) suggested that the luminosity function was well approximated by Equation (2) from -2.4 to 12 mag. Here, Equation (1) is applied to the data collected with the MU radar from 2009 to 2015, and the luminosity function of the meteors detected by the MU radar is investigated. The data consist of 157043 meteors in total. In the following discussion, we assume that the contributions from meteor showers are negligible.

Panel (a) of Figure 6 illustrates the cumulative number flux against the RCS in units of $\text{h}^{-1} \text{km}^{-2}$. The black dashed line is the distribution assuming that the meteor collecting area is uniformly 86.3 km^2 (a disk of 6° in diameter at 100 km in altitude). The meteor collecting area of the MU radar, however, depends on the RCS, since bright meteors can be detected in the side lobes of the beam (Kero et al., 2011). The dependence of the collecting area on the RCS is derived as follows; The distance from the beam center at 100 km ($R_{100 \text{ km}}$) is derived for each meteor by interpolating or extrapolating the trajectory. The area of $\pi R_{100 \text{ km}}^2$ is calculated. The data are divided into groups in the RCS and the median of the area among each group is adopted as the collecting area as a function of the RCS. The derived collecting area against the RCS is shown in Panel (b) of Figure 6. The cumulative number flux calculated based on the derived collecting area is shown by the red line with the 1σ - and 3σ -uncertainty regions in Figure 6. The cumulative number flux larger than 25 dBsm is highly uncertain. The cumulative number flux peaks out around -25 dBsm simply due to the detection limit. In a

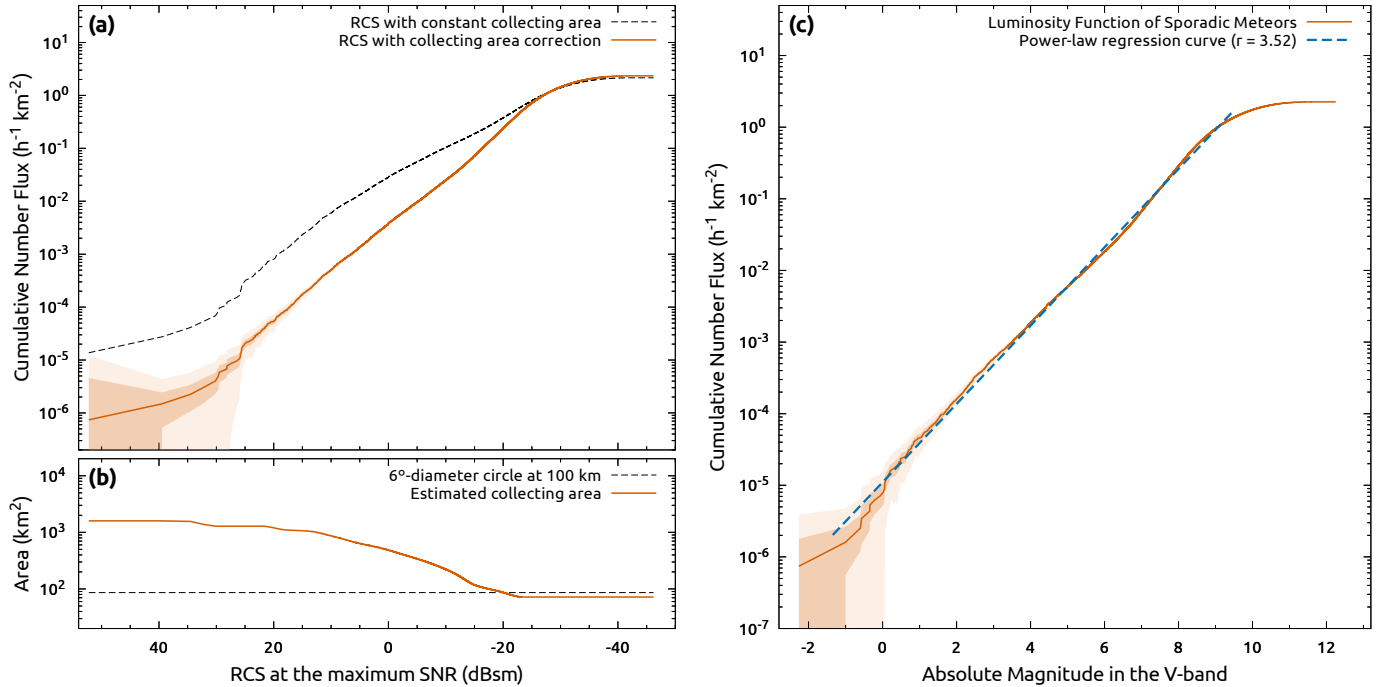


Figure 6: The luminosity function of sporadic meteors. Panel (a) shows the cumulative number flux against the RCS. The black dashed line indicates the number flux assuming that the meteor collecting area does not depend on the RCS. The number flux shown by the red line properly takes into account the dependency. The shaded regions indicate 1σ - and 3σ -level uncertainties. The dependency of the meteor collecting area on the RCS is illustrated in Panel (b) in the red line. The black dashed line is the constant collecting area for reference. Panel (c) shows the luminosity function of sporadic meteors. The uncertainties are the same as in Panel (a). A regression curve is shown by the blue dashed line.

range from -20 to 20 dBsm, the cumulative number flux seems well approximated by a linear function.

The cumulative number flux against the RCS is converted into the luminosity function by applying Equation (1). Panel (c) of Figure 6 illustrates the luminosity function in the red line with the 1σ - and 3σ -uncertainty regions. The luminosity function basically follows an exponential law, which is consistent with previous works (e.g., Hawkins and Upton, 1958; Hawkes and Jones, 1975b; Cook et al., 1980; Ohsawa et al., 2019). The detection limit corresponds to about 10 mag, which is roughly consistent with the detection limit for EISCAT in Pellinen-Wannberg et al. (1998). The population index is derived as $r = 3.52 \pm 0.12$ by fitting a linear function between -1.5 and 9.5 mag, taking into account the systematic uncertainty from Equation (1).

Table 4 lists some population indexes reported in literature. A more detailed overview found in Rendtel (2004). The population indexes have been measured in different methods and different magnitude ranges. As shown in Table 4, there is a considerable variation in the reported population indexes. The present result is roughly consistent with Hawkins (1956b), Kresáková (1966), Cook et al. (1980), and Ohsawa et al. (2019).

Several studies have pointed out the annual and diurnal variations in the population index (e.g., Hughes and Stephenson, 1972; Rendtel, 2004). Panel (a-1) of Figure 7 illustrates the annual variation in the luminosity function. The luminosity functions are normalized around 5 mag.

The annual average of the population index is about 3.49 with a standard deviation of 0.11. Panel (a-2) shows a possible annual variation in the population index: it tends to be high in July–September and low in December–March. Rendtel (2004), however, suggested that the population index increases (decreases) in winter (summer) in the northern hemisphere, which is the opposite to the present result. A similar trend was also reported by Štohl (1976). Rendtel (2004) compiled the dataset from observations in 1998–2003 and the observations in Štohl (1976) were in 1944–1950. The present data were collected 2009–2015. This could be explained in case that the trend in the population index changed in the timescale of decades. Limiting magnitudes in Štohl (1976) and Rendtel (2004) were about 4 and 6 mag, respectively. Instead, the present result is biased toward meteors in a magnitude range of 4–8 mag. This humbly implies that brighter and fainter parts of the luminosity function show different annual variations.

Panel (b-1) of Figure 7 shows the diurnal variation in the luminosity function, normalized as in Panel (a-1). All the times are in the local time (Japan Standard Time). Panel (b-2) shows a diurnal variation in the population index. The averaged population index is 3.33 with a standard deviation of 0.21, suggesting the diurnal variation is more significant than the annual variation. The population index almost constantly decreases from 21:00 and reaches a minimum around 09:00. This trend is roughly consistent with Hughes and Stephenson (1972) and Rendtel (2004),

Table 4: The population indexes in literature

Reference	r -index	s -index	Comment
Hawkins and Upton (1958)	~ 3.45	~ 2.34	-2-3 mag, photographic
Kresáková (1966)	3.5	2.35	-4-6 mag, 21996 visual meteors
Hughes and Stephenson (1972)	—	2.04 ± 0.04	30000 HF radar echoes
Clifton (1973)	~ 3.17	~ 2.252	7-11 mag, TV observation
Hughes (1974)	3.73 ± 0.07	2.43 ± 0.02	-6-0 mag, 10287 visual meteors
Hawkes and Jones (1975b)	—	2.02 ± 0.04	3-7 mag, TV observation
Štohl (1976)	3.70	—	12867 visual meteors
Cook et al. (1980)	3.41	2.335	7-12 mag, phototubes
Rendtel (2004)	2.95 ± 0.06	2.17 ± 0.03	301499 visual meteors, IMO VMDB
Ohsawa et al. (2019)	3.1 ± 0.4	—	3-9 mag, video-rate magnitude
The present result	3.52 ± 0.12	2.46 ± 0.09	0-9 mag, MURMHED

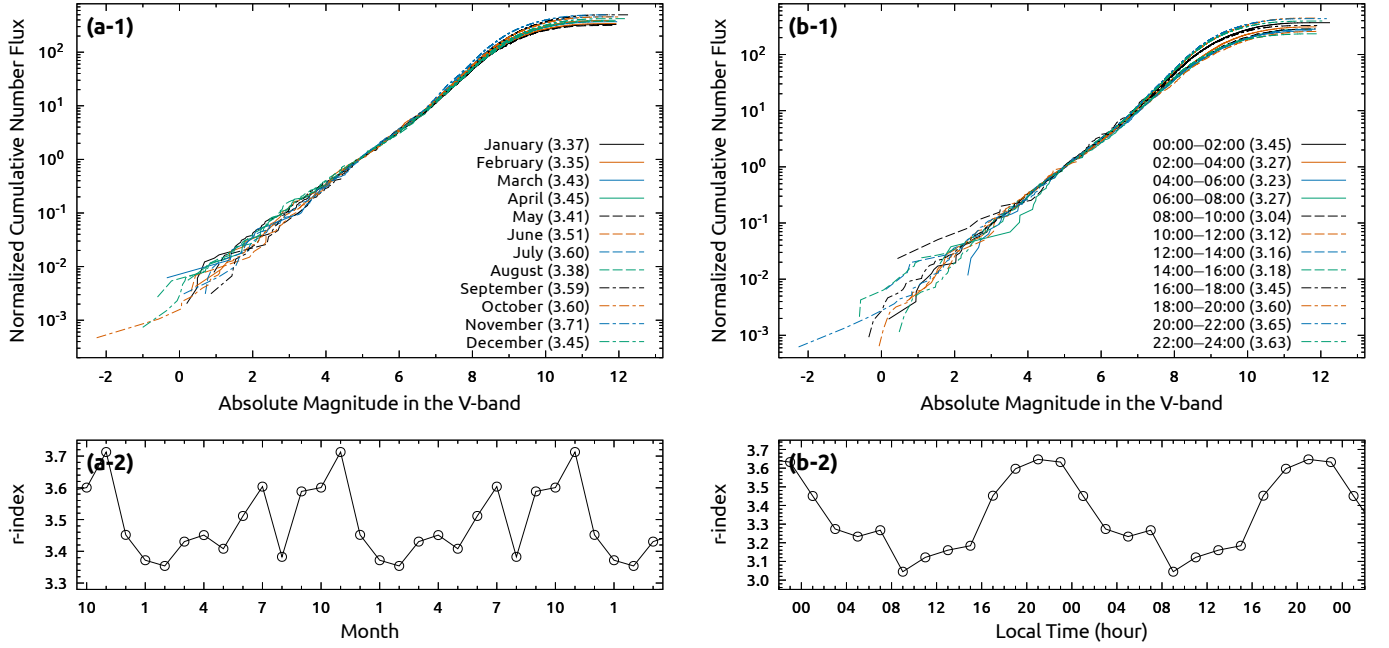


Figure 7: Panel (a-1) shows the month-by-month variation in the luminosity functions, while the diurnal variation in the luminosity functions is shown in Panel (b-1). All the luminosity functions are normalized around 5 mag. The numbers in the legends of each panel indicate the population indexes. The annual and diurnal variations in the population index are shown in Panels (a-2) and (b-2), respectively. The times are based on the detection time stamps in the local time (Japan Standard Time).

although Štohl (1976) reported an almost constant population index in this period. The present result suggests that the diurnal variation in the luminosity function does not depend on the optical magnitude, or the meteoroid mass.

Note that the present population index is heavily dependent on Equation (1). In the discussion above, we naively assume that the relationship between the RCS and the magnitude is constant. The results could be affected by any possible annual or diurnal variations in the relationship. Figure 4 indicates that a large part of the meteors simultaneously detected by radar and optically were attributed to the antihelion and north toroidal sources. The meteors from these sources are typically slower than those from the apex sources, which are dominant in the radar observation (Kero et al., 2012a). Thus, the meteors which were used to derive Equation (1) could be biased toward a larger part of the meteor population. Part of the diurnal variation can be attributable to such an observational bias. More systematic observations are required to examine the validity of the present results.

The optical magnitude is converted into mass using the ablation equations (e.g., Hawkes and Jones, 1975a; Ceplecha et al., 1998). When a meteoroid enters the atmosphere, it is decelerated and heated through interactions with atmospheric constitutions. The meteoroid loses its kinetic energy by decreasing both its mass and velocity. Part of the lost energy is converted into light and observed in optical. The fraction of the meteoroid’s kinetic energy which is converted into light is called the luminous efficiency. The thermal ablation of a meteoroid is calculated following the procedure given by Hill et al. (2005). The parameters in the ablation equations are adopted from Hill et al. (2005). A typical molecular mass and bulk density are respectively set to 50 amu and 3300 kg m^{-3} . The calculation ends when the meteoroid loses 99.999% of the initial mass. The brightest magnitudes are calculated using the normal luminous equation for different meteoroid masses ($10^1, 10^0, \dots, 10^{-7} \text{ g}$), radiant zenith angles ($0, 30^\circ, 45^\circ, 60^\circ, \text{ and } 90^\circ$), and initial velocities ($10, 20, \dots, 70 \text{ km/s}$). The luminous efficiency is taken from Hill et al. (2005), but scaled by 0.081^6 as described in Weryk and Brown (2013). Then, a relationship to calculate the meteoroid mass from the magnitude, velocity, and radiant zenith angle is approximated by the following function:

$$\log_{10} m = 2.76 - 0.38M_V - 2.31 \log_{10} V_\infty - 1.07 \log_{10} \cos z, \quad (3)$$

where m is the mass in units of g , M_V is the optical magnitude, V_∞ is the incident velocity in units of km s^{-1} , and z is the zenith angle of the radiant point. V_∞ and z are calculated from the trajectories measured by the MU radar.

⁶The scaling factor in Weryk and Brown (2013) is 0.453×0.28 , which was optimized to the observation in the R -band. It is further multiplied by 0.638 , which is the band width ration of V -band to the R -band.

The deviation from Equation (3) is typically up to about 0.2 dex . The derived mass depends on the selection of a luminous coefficient. While the current calculation uses the scaled luminous coefficient of Hill et al. (2005), larger luminous coefficients were reported by Ceplecha and Revelle (2005) and Weryk and Brown (2013). If we adopt those luminous coefficients, the derived mass could be smaller by about an order of magnitude.

The cumulative mass distribution, or the mass function, is illustrated in Figure 8. The mass function peaks out around 10^{-5} g , which is attributed to the mass detection limit. The mass function is expected to follow a power-law function:

$$\log_{10} N(>m) = \log_{10} N_1 - (s - 1) \log_{10} m, \quad (4)$$

where m is the meteoroid mass in units of g , $N(>m)$ and N_1 are the event rates of meteors larger than m and 1 g , respectively, and s defines the slope of the mass function, referred as to *the mass index*. The derived regression curve is shown by the blue line. Some mass indexes in literature are listed in Table 4. The mass function deviates from the regression curve around 10^{-4} g . This deviation is likely not a real feature, but could be attributed to the observational bias: the detection limit is given by the RCS rather than the meteoroid mass. The derived mass index is 2.46 ± 0.09 . This value is similar to that in Hughes (1974) and Cook et al. (1980). The mass flux to the Earth in the mass range of 10^{-5} – 10^0 g is about $3 \times 10^3 \text{ kg day}^{-1}$. Ceplecha (1992) provided an incremental mass flux of interplanetary bodies by compiling several observational researches. By integrating it from 10^{-5} to 10^0 g , the mass flux was $1 \times 10^3 \text{ kg day}^{-1}$, which is roughly coincident with our estimation. Love and Brownlee (1993), however, estimated the mass flux in the similar mass range to be about $1 \times 10^5 \text{ kg day}^{-1}$ from the examinations of impact craters on the Long Duration Exposure Facility satellite. The current estimate is more than an order smaller than their estimate. Note that the estimated mass flux depends on the selection of the luminous efficiency. The mass flux will be smaller if the luminous efficiencies of Ceplecha and Revelle (2005) and Weryk and Brown (2013) are applied.

5. Conclusion

We report the results of the two radar-and-optical simultaneous observations of faint meteors. The first observation run was in 2009–2010, using Middle and Upper Atmosphere Radar (MU radar) and an image-intensified CCD video camera equipped with a Canon 200 mm F/1.8 lens. In total, 103 simultaneous sporadic meteors were detected and a typical magnitude was about 6.2 mag . The second observation run was carried out in 2018, using the MU radar and a mosaic CMOS camera, Tomo-e Gozen, installed in the 1.05-m Kiso Schmidt telescope. Consequently, 228 simultaneous sporadic meteors were detected.

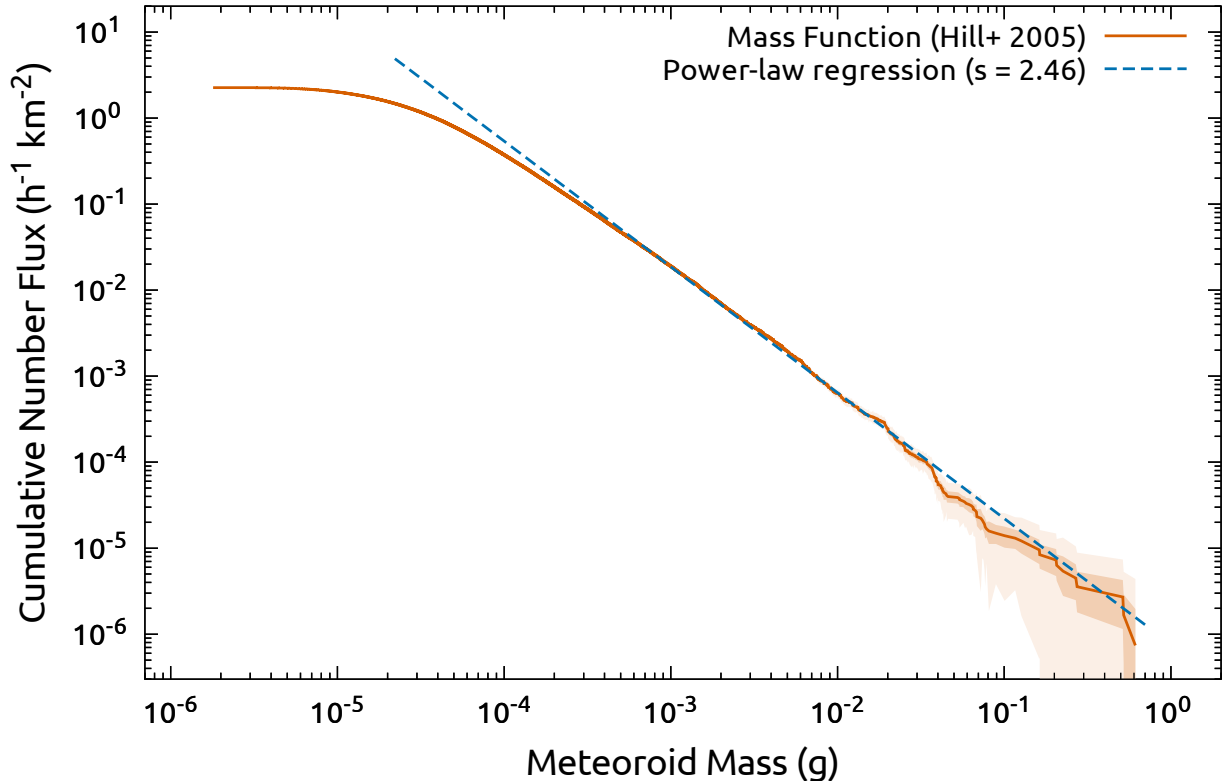


Figure 8: The mass function of sporadic meteors is shown by the red line. The 1σ - and 3σ -level uncertainties are shown by the shaded regions. The blue dashed line indicates the regression curve.

A typical magnitude was about 8.1 mag. The velocity distribution of the detected meteors was bimodal. No apparent trend was found in the altitude and velocity of the meteor in terms of the optical brightness. The distribution of the radiant points indicates that the fast ($> 45 \text{ km s}^{-1}$) and slow ($\leq 45 \text{ km s}^{-1}$) populations are attributed to the apex sources and the antihelion or north-toroidal sources, respectively.

The optical magnitude calibrated to the V -band linearly decreased with increasing radar cross section (RCS) at the peak signal-to-noise ratio. The linear regression line was derived as: $M_V = (-0.169 \pm 0.006) \times A + (4.43 \pm 0.13)$, where M_V is the V -band magnitude and A is the RCS in units of dBsm. The slope of the regression line was marginally consistent with that in Nishimura et al. (2001). The slope in Brown et al. (2017), which was obtained in a magnitude range of 0–6 mag, was smaller than the present result. Further observations are required to investigate the difference in the slopes. Although there is large scatter around the regression line, we confidently obtained a conversion function from the RCS to the optical magnitude.

By applying the derived conversion function to more than 150,000 meteors collected from the MU Radar Meteor Head Echo Database (MURMHED), we compile a luminosity function of faint sporadic meteors in units of $\text{hour}^{-1} \text{ km}^{-2}$. The luminosity function is well approximated by an exponential function in a magnitude range

of -1.5 – 9.5 mag. The population index r is constrained to be 3.52 ± 0.12 by fitting the exponential function. The luminosity function peaks out around 10 mag, corresponding to the detection limit of the MU radar. The annual and diurnal variations in the luminosity function are investigated. The present result shows the opposite trend to the trends in literature (Štohl, 1976; Rendtel, 2004). This is possibly explained by assuming the trend changes in a timescale of decades or that the trend depends on the optical magnitude. The present diurnal variation is consistent with previous works, suggesting that the diurnal variation is less dependent on the optical magnitude. The optical magnitude was converted into the mass of the meteoroid based on the thermal ablation theory and the luminous efficiency in Hill et al. (2005) but scaled by 0.081 as described in Weryk and Brown (2013). The size index s is constrained to be 2.46 ± 0.09 by fitting a power-law function. The mass function peaks out around 10^{-5} g. We conclude that the MU radar is able to detect interplanetary particles of 10^{-5} – 10^0 g in mass as meteors. The mass flux to the Earth in this mass range is estimated to be a few 10^3 kg day^{-1} , but this amount could suffer from the uncertainty in the luminous efficiency.

The present results are based on the relationship between the RCS and the optical magnitude. This is derived from the two observation runs, which were conducted with the different observing systems and in the different seasons. The derived relationship is possibly affected by

systematic errors which are not taken into account in the current analysis. Further systematic observations are required to validate the present results. The combination of the MU radar and Tomo-e Gozen seems promising to conduct such observations and to investigate statistical characteristics of faint meteors.

Acknowledgments

This research has been partly supported by Japan Society for the Promotion of Science (JSPS) Grants-in-Aid for Scientific Research (KAKENHI) Grant Numbers 26287106, 16H02158, 16H06341, 18H01272, 18H01261, 18H04575, and 18K13599. This research is also supported in part by the Japan Science and Technology (JST) Agency's Pre-cursory Research for Embryonic Science and Technology (PRESTO), the Research Center for the Early Universe (RESCEU), of the School of Science at the University of Tokyo, and the Optical and Near-infrared Astronomy Inter-University Cooperation Program. The meteor head echo data (MURMHED) used in this study have been created by T. Nakamura (NIPR, Japan), J. Kero (IRF, Sweden) and members of the radar meteor head echo database group under the support by JSPS Grant-in-Aid for Publication of Scientific Research Results (KAKENHI Databases) Grant Number 258033. The MU radar belongs to and is operated by RISH (Research Institute of Sustainable Humankind), Kyoto University.

References

- Andreć, Ž., Gural, P., Šegon, D., Skokić, I., Korlević, K., Vida, D., Novoselnik, F., Gostinski, D., 2014. Results of CMN 2013 search for new showers across CMN and SonotaCo databases I-0.5mm. WGN, Journal of the International Meteor Organization 42, 90–97.
 URL <http://adsabs.harvard.edu/abs/2014JIMO...42...90A>
- Andreć, Ž., Šegon, D., Korlević, K., Novoselnik, F., Vida, D., Skokić, I., 2013. Ten possible new showers from the Croatian Meteor Network and SonotaCo datasets. WGN, Journal of the International Meteor Organization 41, 103–108.
 URL <http://adsabs.harvard.edu/abs/2013JIMO...41..103A>
- Baldwin, B., Sheaffer, Y., 1971. Ablation and breakup of large meteoroids during atmospheric entry. Journal of Geophysical Research 76, 4653.
 URL <https://ui.adsabs.harvard.edu/abs/1971JGR...76.4653B/abstract>
- Boitnott, C. A., Savage, H. F., 1972. Light-Emission Measurements of Iron at Simulated Meteor Conditions. The Astrophysical Journal 174, 201.
 URL <http://adsabs.harvard.edu/abs/1972ApJ...174..201B>
- Brown, P., Stober, G., Schult, C., Krzeminski, Z., Cooke, W., Chau, J. L., 2017. Simultaneous optical and meteor head echo measurements using the Middle Atmosphere Alomar Radar System (MAARSY): Data collection and preliminary analysis. Planetary and Space Science 141, 25–34.
 URL <https://ui.adsabs.harvard.edu/abs/2017P%26SS...141...25B/abstract>
- Campbell-Brown, M. D., Borovička, J., Brown, P. G., Stokan, E., 2013. High-resolution modelling of meteoroid ablation. Astronomy and Astrophysics 557, A41.
 URL <http://adsabs.harvard.edu/abs/2013A%26A...557A..41C>
- Campbell-Brown, M. D., Kero, J., Szasz, C., Pellinen-Wannberg, A., Weryk, R. J., 2012. Photometric and ionization masses of meteors with simultaneous EISCAT UHF radar and intensified video observations. Journal of Geophysical Research (Space Physics) 117 (A9), A09323.
 URL <https://ui.adsabs.harvard.edu/abs/2012JGRA...117.9323C/abstract>
- Ceplecha, Z., 1992. Influx of interplanetary bodies onto earth. Astronomy and Astrophysics 263, 361–366.
 URL <http://adsabs.harvard.edu/abs/1992A%26A...263..361C>
- Ceplecha, Z., Borovička, J., Elford, W. G., Revelle, D. O., Hawkes, R. L., Porubčan, V., Šimek, M., 1998. Meteor Phenomena and Bodies. Space Science Reviews 84, 327–471.
 URL <https://ui.adsabs.harvard.edu/abs/1998SSRv...84..327C/abstract>
- Ceplecha, Z., Revelle, D. O., 2005. Fragmentation model of meteoroid motion, mass loss, and radiation in the atmosphere. Meteoritics and Planetary Science 40 (1), 35.
 URL <http://adsabs.harvard.edu/abs/2005M%26PS...40...35C>
- Clifton, K. S., 1973. Television studies of faint meteors. Journal of Geophysical Research 78, 6511.
 URL <https://ui.adsabs.harvard.edu/abs/1973JGR...78.6511C/abstract>
- Close, S., Brown, P., Campbell-Brown, M., Oppenheim, M., Colestock, P., 2007. Meteor head echo radar data: Mass-velocity selection effects. Icarus 186, 547–556.
 URL <https://ui.adsabs.harvard.edu/abs/2007Icar...186.547C/abstract>
- Close, S., Hunt, S. M., Minardi, M. J., McKeen, F. M., 2000. Analysis of Perseid meteor head echo data collected using the Advanced Research Projects Agency Long-Range Tracking and Instrumentation Radar (ALTAIR). Radio Science 35, 1233.
 URL <https://ui.adsabs.harvard.edu/abs/2000RaSc...35.1233C/abstract>
- Close, S., Oppenheim, M., Durand, D., Dyrud, L., 2005. A new method for determining meteoroid mass from head echo data. Journal of Geophysical Research (Space Physics) 110, A09308.
 URL <http://adsabs.harvard.edu/abs/2005JGRA...110.9308C>
- Close, S., Oppenheim, M., Hunt, S., Coster, A., 2004. A technique for calculating meteor plasma density and meteoroid mass from radar head echo scattering. Icarus 168, 43–52.
 URL <http://adsabs.harvard.edu/abs/2004Icar...168...43C>
- Cook, A. F., Weekes, T. C., Williams, J. T., Omongain, E., 1980. Flux of optical meteors down to MPG = +12. Monthly Notices of the Royal Astronomical Society 193, 645–666.
 URL <https://ui.adsabs.harvard.edu/abs/1980MNRAS...193.645C/abstract>
- Fentzke, J. T., Janches, D., Sparks, J. J., 2009. Latitudinal and seasonal variability of the micrometeor input function: A study using model predictions and observations from Arecibo and PFISR. Journal of Atmospheric and Solar-Terrestrial Physics 71, 653–661.
 URL <https://ui.adsabs.harvard.edu/abs/2009JASTP...71.653F/abstract>
- Flynn, G. J., 2002. Extraterrestrial Dust in the Near-Earth Environment. In: Meteors in the Earth's Atmosphere. p. 77.
 URL <https://ui.adsabs.harvard.edu/abs/2002mea...book...77F/abstract>
- Friichtenicht, J. F., Becker, D. G., 1973. Determination of Meteor Parameters Using Laboratory Simulation Techniques. NASA Special Publication 319, 53.
 URL <http://adsabs.harvard.edu/abs/1973NASSP.319...53F>
- Fujiwara, Y., Ueda, M., Nakamura, T., Tsutsumi, M., 1995. Simultaneous Observations of Meteors with the Radar and TV Systems. Earth Moon and Planets 68, 277–282.
 URL <https://ui.adsabs.harvard.edu/abs/1995EM%26P...68.277F/abstract>
- Gruen, E., Fechtig, H., Kissel, J., Linkert, D., Maas, D., McDonnell, J. A. M., Morfill, G. E., Schwehm, G., Zook, H. A., Giese, R. H., 1992. The ULYSSES dust experiment. Astronomy and Astrophysics Supplement Series 92, 411–423.

- URL <https://ui.adsabs.harvard.edu/abs/1992A%26AS...92..411G/abstract>
- Grün, E., Zook, H. A., Fechtig, H., Giese, R. H., 1985. Collisional balance of the meteoritic complex. *Icarus* 62, 244–272.
URL <https://ui.adsabs.harvard.edu/abs/1985Icar...62..244G/abstract>
- Gural, P., Šegon, D., Andreić, Ž., Skokić, I., Korlević, K., Vida, D., Novoselnik, F., Gostinski, D., 2014. Results of CMN 2013 search for new showers across CMN and SonotaCo databases II. WGN, *Journal of the International Meteor Organization* 42, 132–138.
URL <http://adsabs.harvard.edu/abs/2014JIMO...42..132G>
- Gurnett, D. A., Ansher, J. A., Kurth, W. S., Granroth, L. J., 1997. Micron-sized dust particles detected in the outer solar system by the Voyager 1 and 2 plasma wave instruments. *Geophysical Research Letters* 24, 3125–3128.
URL <https://ui.adsabs.harvard.edu/abs/1997GeoRL...24..3125G/abstract>
- Hawkes, R. L., Jones, J., 1975a. A quantitative model for the ablation of dustball meteors. *Monthly Notices of the Royal Astronomical Society* 173, 339–356.
URL <https://ui.adsabs.harvard.edu/abs/1975MNRAS.173..339H/abstract>
- Hawkes, R. L., Jones, J., 1975b. Television observations of faint meteors. I - Mass distribution and diurnal rate variation. *Monthly Notices of the Royal Astronomical Society* 170, 363–377.
URL <https://ui.adsabs.harvard.edu/abs/1975MNRAS.170..363H/abstract>
- Hawkins, G. S., 1956a. A radio echo survey of sporadic meteor radiants. *Monthly Notices of the Royal Astronomical Society* 116, 92.
URL <https://ui.adsabs.harvard.edu/abs/1956MNRAS.116...92H/abstract>
- Hawkins, G. S., 1956b. Variation in the occurrence rate of meteors. *The Astronomical Journal* 61, 386.
URL <https://ui.adsabs.harvard.edu/abs/1956AJ....61..386H/abstract>
- Hawkins, G. S., Upton, E. K. L., 1958. The Influx Rate of Meteors in the Earth's Atmosphere. *The Astrophysical Journal* 128, 727.
URL <https://ui.adsabs.harvard.edu/abs/1958ApJ...128..727H/abstract>
- Hill, K. A., Rogers, L. A., Hawkes, R. L., 2005. High geocentric velocity meteor ablation. *Astronomy and Astrophysics* 444, 615–624.
URL <http://adsabs.harvard.edu/abs/2005A%26A...444..615H>
- Hughes, D. W., 1974. The influx of visual sporadic meteors. *Monthly Notices of the Royal Astronomical Society* 166, 339.
URL <https://ui.adsabs.harvard.edu/abs/1974MNRAS.166..339H/abstract>
- Hughes, D. W., Stephenson, D. G., 1972. The diurnal variation in the massdistribution of sporadic meteors. *Monthly Notices of the Royal Astronomical Society* 155, 403.
URL <https://ui.adsabs.harvard.edu/abs/1972MNRAS.155..403H/abstract>
- Iye, M., Tanaka, M., Yanagisawa, M., Ebizuka, N., Ohnishi, K., Hirose, C., Asami, N., Komiyama, Y., Furusawa, H., 2007. SuprimeCam Observation of Sporadic Meteors during Perseids 2004. *Publications of the Astronomical Society of Japan* 59, 841–855.
URL <https://ui.adsabs.harvard.edu/abs/2007PASJ...59..841I/abstract>
- Janches, D., Brunini, C., Hormaechea, J. L., 2019. A Decade of Sporadic Meteoroid Mass Distribution Indices in the Southern Hemisphere Derived from SAAMER's Meteor Observations. *The Astronomical Journal* 157 (6), 240.
URL <http://adsabs.harvard.edu/abs/2019AJ....157..240J>
- Janches, D., Close, S., Hormaechea, J. L., Swarnalingam, N., Murphy, A., O'Connor, D., Vandepeer, B., Fuller, B., Fritts, D. C., Brunini, C., 2015. The Southern Argentina Agile MEteor Radar Orbital System (SAAMER-OS): An Initial Sporadic Meteoroid Orbital Survey in the Southern Sky. *The Astrophysical Journal* 809, 36.
URL <https://ui.adsabs.harvard.edu/abs/2015ApJ...809...36J/abstract>
- Janches, D., Hocking, W., Pifko, S., Hormaechea, J. L., Fritts, D. C., Brunini, C., Michell, R., Samara, M., 2014. Interferometric meteor head echo observations using the Southern Argentina Agile Meteor Radar. *Journal of Geophysical Research (Space Physics)* 119, 2269–2287.
URL <http://adsabs.harvard.edu/abs/2014JGRA...119.2269J>
- Jenniskens, P., 2017. Meteor showers in review. *Planetary and Space Science* 143, 116–124.
URL <http://www.sciencedirect.com/science/article/pii/S0032063316303579>
- Jenniskens, P., Gural, P. S., Dynneson, L., Grigsby, B. J., Newman, K. E., Borden, M., Koop, M., Holman, D., 2011. CAMS: Cameras for Allsky Meteor Surveillance to establish minor meteor showers. *Icarus* 216, 40.
URL <https://ui.adsabs.harvard.edu/abs/2011Icar...216...40J/abstract>
- Jenniskens, P., Nénon, Q., 2016. CAMS verification of single-linked high-threshold D-criterion detected meteor showers. *Icarus* 266, 371–383.
URL <https://ui.adsabs.harvard.edu/abs/2016Icar...266..371J/abstract>
- Jones, W., 1997. Theoretical and observational determinations of the ionization coefficient of meteors. *Monthly Notices of the Royal Astronomical Society* 288, 995.
URL <https://ui.adsabs.harvard.edu/abs/1997MNRAS.288..995J/abstract>
- Kanamori, T., 2009. A meteor shower catalog based on video observations in 2007–2008. WGN, *Journal of the International Meteor Organization* 37, 55.
URL <https://ui.adsabs.harvard.edu/abs/2009JIMO...37...55K/abstract>
- Kero, J., Szasz, C., Nakamura, T., Meisel, D. D., Ueda, M., Fujiwara, Y., Terasawa, T., Miyamoto, H., Nishimura, K., 2011. First results from the 2009–2010 MU radar head echo observation programme for sporadic and shower meteors: the Orionids 2009. *Monthly Notices of the Royal Astronomical Society* 416, 2550–2559.
URL <https://ui.adsabs.harvard.edu/abs/2011MNRAS.416.2550K/abstract>
- Kero, J., Szasz, C., Nakamura, T., Meisel, D. D., Ueda, M., Fujiwara, Y., Terasawa, T., Nishimura, K., Watanabe, J., 2012a. The 2009–2010 MU radar head echo observation programme for sporadic and shower meteors: radiant densities and diurnal rates. *Monthly Notices of the Royal Astronomical Society* 425 (1), 135–146.
URL <https://ui.adsabs.harvard.edu/abs/2012MNRAS.425..135K/abstract>
- Kero, J., Szasz, C., Nakamura, T., Terasawa, T., Miyamoto, H., Nishimura, K., 2012b. A meteor head echo analysis algorithm for the lower VHF band. *Annales Geophysicae* 30 (4), 639.
URL <https://ui.adsabs.harvard.edu/abs/2012AnGeo...30..639K/abstract>
- Kero, J., Szasz, C., Pellinen-Wannberg, A., Wannberg, G., Westman, A., Meisel, D. D., 2008. Three-dimensional radar observation of a submillimeter meteoroid fragmentation. *Geophysical Research Letters* 35, L04101.
URL <http://adsabs.harvard.edu/abs/2008GeoRL...35.4101K>
- Kojima, Y., Sako, S., Ohsawa, R., Takahashi, H., Doi, M., Kobayashi, N., Aoki, T., Arima, N., Arimatsu, K., Ichiki, M., Ikeda, S., Inooka, K., Ita, Y., Kasuga, T., Kokubo, M., Konishi, M., Maehara, H., Matsunaga, N., Mitsuda, K., Miyata, T., Mori, Y., Morii, M., Morokuma, T., Motohara, K., Nakada, Y., Okumura, S.-I., Sarugaku, Y., Sato, M., Shigeyama, T., Soyano, T., Tanaka, M., Tarusawa, K., Tominaga, N., Totani, T., Urakawa, S., Usui, F., Watanabe, J., Yamashita, T., Yoshikawa, M., 2018. Evaluation of large pixel CMOS image sensors for the Tomoe Gozen wide field camera. In: *Proc. SPIE. Vol. 10709. International Society for Optics and Photonics*, p. 107091T.
URL <https://doi.org/10.1117/12.2311301>

- Kornos, L., Koukal, J., Piff, R., Toth, J., 2013. Database of meteoroid orbits from several European video networks. In: Proceedings of the 31st International Meteor Conference. The International Meteor Organization, pp. 21–25.
URL <https://ui.adsabs.harvard.edu/abs/2013pimo.conf...21K/abstract>
- Kresáková, M., 1966. The Magnitude Distribution of Meteors in Meteor Streams. Contributions of the Astronomical Observatory Skalnaté Pleso 3, 75.
URL <https://ui.adsabs.harvard.edu/abs/1966CoSka...3...75K/abstract>
- Love, S. G., Brownlee, D. E., 1993. A Direct Measurement of the Terrestrial Mass Accretion Rate of Cosmic Dust. *Science* 262, 550–553.
URL <http://adsabs.harvard.edu/abs/1993Sci...262..550L>
- Michell, R. G., 2010. Simultaneous optical and radar measurements of meteors using the Poker Flat Incoherent Scatter Radar. *Journal of Atmospheric and Solar-Terrestrial Physics* 72 (16), 1212–1220.
URL <https://ui.adsabs.harvard.edu/abs/2010JASTP...72.1212M/abstract>
- Michell, R. G., DeLuca, M., Janches, D., Chen, R., Samara, M., 2019. Simultaneous optical and dual-frequency radar observations of small mass meteors at Arecibo. *Planetary and Space Science* 166, 1–8.
URL <http://adsabs.harvard.edu/abs/2019P%26SS...166...1M>
- Michell, R. G., Janches, D., Samara, M., Hormaechea, J. L., Brunini, C., Bibbo, I., 2015. Simultaneous optical and radar observations of meteor head-echoes utilizing SAAMER. *Planetary and Space Science* 118, 95–101.
URL <https://ui.adsabs.harvard.edu/abs/2015P%26SS...118...95M/abstract>
- Myers, J. R., Sande, C. B., Miller, A. C., Warren, W. H., Tracewell, D. A., 2001. VizieR Online Data Catalog: SKY2000 Catalog, Version 4 (Myers+ 2002). VizieR Online Data Catalog, V/109.
URL <https://ui.adsabs.harvard.edu/abs/2001yCat.5109...0M/abstract>
- Nishimura, K., Sato, T., Nakamura, T., Ueda, M., 2001. High sensitivity radar-optical observations of faint meteors. *IEICE Transactions on Electronics E84-C* (12), 1877–1884.
- Nishimura, S., Ohnishi, K., Dobashi, K., Watanabe, J.-I., Miyata, T., Nakada, Y., 2002. Optical Imaging of the Radiant Points of Leonids during the 2001 Storm with the 105cm Kiso Schmidt Telescope. *Publications of the Astronomical Society of Japan* 54, L83–L88.
URL <https://ui.adsabs.harvard.edu/abs/2002PASJ...54L..83N/abstract>
- Ohsawa, R., Sako, S., Sarugaku, Y., Usui, F., Ootsubo, T., Fujiwara, Y., Sato, M., Kasuga, T., Arimatsu, K., Watanabe, J.-i., Doi, M., Kobayashi, N., Takahashi, H., Motohara, K., Morokuma, T., Konishi, M., Aoki, T., Soyano, T., Tarusawa, K., Mori, Y., Nakada, Y., Ichiki, M., Arima, N., Kojima, Y., Morita, M., Shigeyama, T., Ita, Y., Kokubo, M., Mitsuda, K., Maehara, H., Tominaga, N., Yamashita, T., Ikeda, S., Morii, M., Urakawa, S., Okumura, S.-i., Yoshikawa, M., 2019. Luminosity function of faint sporadic meteors measured with a wide-field CMOS mosaic camera Tomo-e PM. *Planetary and Space Science* 165, 281–292.
URL <https://ui.adsabs.harvard.edu/abs/2019P%26SS...165..281O/abstract>
- Ohsawa, R., Sako, S., Takahashi, H., Kikuchi, Y., Doi, M., Kobayashi, N., Aoki, T., Arimatsu, K., Ichiki, M., Ikeda, S., Ita, Y., Kasuga, T., Kawakita, H., Kokubo, M., Maehara, H., Matsunaga, N., Mito, H., Mitsuda, K., Miyata, T., Mori, K., Mori, Y., Morii, M., Morokuma, T., Motohara, K., Nakada, Y., Okumura, S.-i., Onozato, H., Osawa, K., Sarugaku, Y., Sato, M., Shigeyama, T., Soyano, T., Tanaka, M., Taniguchi, Y., Tanikawa, A., Tarusawa, K., Tominaga, N., Totani, T., Urakawa, S., Usui, F., Watanabe, J., Yamaguchi, J., Yoshikawa, M., 2016. Development of a real-time data processing system for a prototype of the Tomo-e Gozen wide field CMOS camera. In: Proc. SPIE. Vol. 9913. International Society for Optics and Photonics, p. 991339.
URL <http://proceedings.spiedigitallibrary.org/proceeding.aspx?articleid=2543636>
- Pellinen-Wannberg, A., Wannberg, G., 1994. Meteor observations with the European incoherent scatter UHF radar. *Journal of Geophysical Research* 99, 11379.
URL <https://ui.adsabs.harvard.edu/1994JGR...9911379P/abstract>
- Pellinen-Wannberg, A., Westman, A., Wannberg, G., Kaila, K., 1998. Meteor fluxes and visual magnitudes from EISCAT radar event rates: a comparison with cross-section based magnitude estimates and optical data. *Annales Geophysicae* 16 (11), 1475–1485.
URL <https://www.ann-geophys.net/16/1475/1998/>
- Plane, J. M. C., 2012. Cosmic dust in the earth's atmosphere. *Chemical Society Reviews*, Vol. 41, p. 6507–6518, 2012 41, 6507–6518.
URL <https://ui.adsabs.harvard.edu/abs/2012ChSRv...41.6507P/abstract>
- Popova, O., 2004. Meteoroid ablation models. *Earth Moon and Planets* 95, 303–319.
URL <https://ui.adsabs.harvard.edu/abs/2004EM%26P...95..303P/abstract>
- Rendtel, J., 2004. The population index of sporadic meteors. In: Proceedings of the 22nd International Meteor Conference. Vol. 22. Bollmannsruh, Germany, pp. 114–122.
URL <https://ui.adsabs.harvard.edu/abs/2004pimo.conf...114R/abstract>
- Saidov, K. H., Simek, M., 1989. Luminous Efficiency Coefficient from Simultaneous Meteor Observations. *Bulletin of the Astronomical Institutes of Czechoslovakia* 40, 330.
URL <https://ui.adsabs.harvard.edu/1989BAICz...40..330S/abstract>
- Sako, S., Ohsawa, R., Takahashi, H., Kikuchi, Y., Doi, M., Kobayashi, N., Aoki, T., Arimatsu, K., Ichiki, M., Ikeda, S., Ita, Y., Kasuga, T., Kawakita, H., Kokubo, M., Maehara, H., Matsunaga, N., Mito, H., Mitsuda, K., Miyata, T., Mori, K., Mori, Y., Morii, M., Morokuma, T., Motohara, K., Nakada, Y., Osawa, K., Okumura, S.-i., Onozato, H., Sarugaku, Y., Sato, M., Shigeyama, T., Soyano, T., Tanaka, M., Taniguchi, Y., Tanikawa, A., Tarusawa, K., Tominaga, N., Totani, T., Urakawa, S., Usui, F., Watanabe, J., Yamaguchi, J., Yoshikawa, M., 2016. Development of a prototype of the Tomo-e Gozen wide-field CMOS camera. In: Proc. SPIE. Vol. 9908. International Society for Optics and Photonics, p. 99083P.
URL <http://proceedings.spiedigitallibrary.org/proceeding.aspx?articleid=2544194>
- Sako, S., Ohsawa, R., Takahashi, H., Kojima, Y., Doi, M., Kobayashi, N., Aoki, T., Arima, N., Arimatsu, K., Ichiki, M., Ikeda, S., Inooka, K., Ita, Y., Kasuga, T., Kokubo, M., Konishi, M., Maehara, H., Matsunaga, N., Mitsuda, K., Miyata, T., Mori, Y., Morii, M., Morokuma, T., Motohara, K., Nakada, Y., Okumura, S.-i., Sarugaku, Y., Sato, M., Shigeyama, T., Soyano, T., Tanaka, M., Tarusawa, K., Tominaga, N., Totani, T., Urakawa, S., Usui, F., Watanabe, J., Yamashita, T., Yoshikawa, M., 2018. The Tomo-e Gozen wide field CMOS camera for the Kiso Schmidt telescope. In: Proc. SPIE. Vol. 10702. International Society for Optics and Photonics, p. 107020J.
URL <https://doi.org/10.1117/12.2310049>
- Sato, T., Nakamura, T., Nishimura, K., 2000. Orbit Determination of Meteors Using the MU Radar. *IEICE TRANSACTIONS on Communications E83-B* (9), 1990–1995.
URL http://search.ieice.org/bin/summary.php?id=e83-b_9_1990&category=B&year=2000&lang=E&abst=
- Schult, C., Stober, G., Janches, D., Chau, J. L., 2017. Results of the first continuous meteor head echo survey at polar latitudes. *Icarus* 297, 1–13.
URL <http://adsabs.harvard.edu/abs/2017Icar...297....1S>
- Šegon, D., Andreić, Ž., Gural, P., Skokić, I., Korlević, K., Vida, D., Novoselnik, F., Gostinski, D., 2014. Results of CMN 2013 search for new showers across CMN and SonotaCo databases III. *WGN, Journal of the International Meteor Organization* 42, 227–233.
URL <http://adsabs.harvard.edu/abs/2014JIM0...42..227S>

- Southworth, R. B., Hawkins, G. S., 1963. Statistics of meteor streams. *Smithsonian Contributions to Astrophysics* 7, 261.
 URL <https://ui.adsabs.harvard.edu/1963SCoA...7..261S/abstract>
- Sparks, J. J., Janches, D., Nicolls, M. J., Heinselman, C. J., 2009. Seasonal and diurnal variability of the meteor flux at high latitudes observed using PFISR. *Journal of Atmospheric and Solar-Terrestrial Physics* 71, 644–652.
 URL <http://adsabs.harvard.edu/abs/2009JASTP...71..644S>
- Štohl, J., 1968. Seasonal Variation in the Radiant Distribution of Meteors. *Physics and Dynamics of Meteors* 33, 298.
 URL <https://ui.adsabs.harvard.edu/abs/1968IAUS...33..298S/abstract>
- Štohl, J., 1976. The magnitude distribution of sporadic meteors and its variations. *Contributions of the Astronomical Observatory Skalnaté Pleso* 7, 7.
 URL <https://ui.adsabs.harvard.edu/abs/1976CoSka...7...7S/abstract>
- Szalay, J. R., Piquette, M., Horányi, M., 2013. The Student Dust Counter: Status report at 23 AU. *Earth, Planets, and Space* 65, 1145–1149.
 URL <https://ui.adsabs.harvard.edu/abs/2013EP%26S...65.1145S/abstract>
- Thomas, E., Horányi, M., Janches, D., Munsat, T., Simolka, J., Sternovsky, Z., 2016. Measurements of the ionization coefficient of simulated iron micrometeoroids. *Geophysical Research Letters* 43, 3645–3652.
 URL <http://adsabs.harvard.edu/abs/2016GeoRL...43.3645T>
- Verniani, F., 1965. On the Luminous Efficiency of Meteors. *Smithsonian Contributions to Astrophysics* 8, 141.
 URL <http://adsabs.harvard.edu/abs/1965SCoA...8..141V>
- Weryk, R. J., Brown, P. G., 2012. Simultaneous radar and video meteors — I: Metric comparisons. *Planetary and Space Science* 62 (1), 132.
 URL <https://ui.adsabs.harvard.edu/abs/2012P%26SS...62..132W/abstract>
- Weryk, R. J., Brown, P. G., 2013. Simultaneous radar and video meteors — II: Photometry and ionisation. *Planetary and Space Science* 81, 32.
 URL <https://ui.adsabs.harvard.edu/abs/2013P%26SS...81...32W/abstract>
- Weryk, R. J., Campbell-Brown, M. D., Wiegert, P. A., Brown, P. G., Krzeminski, Z., Musci, R., 2013. The Canadian Automated Meteor Observatory (CAMO): System overview. *Icarus* 225 (1), 614–622.
 URL <http://adsabs.harvard.edu/abs/2013Icar...225..614W>
- Zacharias, N., Finch, C. T., Girard, T. M., Henden, A., Bartlett, J. L., Monet, D. G., Zacharias, M. I., 2013. The Fourth US Naval Observatory CCD Astrograph Catalog (UCAC4). *The Astronomical Journal* 145, 44.
 URL <https://ui.adsabs.harvard.edu/2013AJ...145...44Z/abstract>